buildings

MDPI

Article

Structural Performance of Prefabricated Corrugated Steel Plate Retaining Walls in Alpine Permafrost Regions: Numerical Simulation and Experimental Validation

Wei Chen [1,2], Ting Duan [2], Lianxia Ma [1,2], Bailai Liu [3], Xiaofei Jia [3], Fang Chen [2], Yang Lv [4] and Qingtao Zheng [2,4,*]

[1] Xinjiang Key Laboratory of Prefabricated Transportation Construction and Maintenance, Urumqi 830016, China
[2] Xinjiang Communications Construction Group Co., Ltd., Urumqi 830016, China; songpengzhen@longshine.com (T.D.)
[3] Civil & Architecture Engineering, Xi'an Technological University, Xi'an 710021, China
[4] Tianjin Key Laboratory of Civil Structure Protection and Reinforcement, Tianjin Chengjian University, Tianjin 300384, China
* Correspondence: zhengqingtao@tju.edu.cn

Abstract

Alpine permafrost and seasonally frozen ground threaten the long-term safe operation of highway infrastructures. Aiming at the structural performance optimization of prefabricated corrugated steel plate retaining walls in alpine permafrost regions, this study adopted finite element numerical simulation combined with field test validation to systematically explore the influences of wall height, plate thickness, corrugation geometry, and tie reinforcement layout on structural deformation and internal force, and carried out targeted parameter optimization. The core innovations include the following: (1) Structural lateral displacement and internal force rise nonlinearly with the increase in wall height, and high retaining walls exhibit an accelerated growth trend of deformation and stress. (2) Increasing plate thickness can effectively reduce structural displacement and stress, while the improvement effect gradually weakens after exceeding a critical thickness. Specifically, when the thickness increases from 4 mm to 5 mm, the displacement decreases by 33.13%. (3) Appropriately increasing corrugation pitch and height improves structural equivalent stiffness and optimizes stress distribution. Increasing the corrugation pitch from 75 mm to 400 mm and corrugation height from 25 mm to 150 mm reduces the maximum horizontal displacement by 52.6%. This demonstrates that larger corrugation profiles significantly improve structural stiffness. For walls higher than 6 m, the spacing should be reduced to 0.8 m × 1.0 m to provide additional lateral restraint. (4) Furthermore, seasonal freeze–thaw cycles and a non-uniform temperature field significantly amplify structural displacement and stress. After 12 months of freeze–thaw cycles, the maximum horizontal displacement increases by 49.7% and the maximum equivalent stress increases by 56.9% compared to the initial state. This study clarifies the parameter control mechanism and temperature coupling effect and provides a reliable theoretical basis and design reference for the engineering application of prefabricated corrugated steel plate retaining walls in alpine permafrost areas.

Keywords: alpine permafrost regions; prefabricated corrugated steel plate; corrugated steel plate retaining wall; numerical simulation; experimental validation

Academic Editor: Giuseppina Uva

Received: 1 May 2026
Revised: 4 June 2026
Accepted: 5 June 2026
Published: 25 June 2026

1. Introduction

Alpine permafrost and seasonally frozen ground feature strong temperature sensitivity and complex engineering mechanical behaviors. Soil frost heave easily causes the cracking, deformation, and instability of slopes, highway subgrades, and retaining structures. It has become a key factor restricting the construction quality and long-term operation safety of highway engineering in alpine permafrost regions. In highway engineering construction in permafrost regions, the service performance of subgrade retaining walls, as the core retaining structures, directly determines the operational safety of highway lines. Conventional masonry retaining walls have obvious inherent defects. They feature long construction cycles and a poor adaptability to low-temperature environments. They are also prone to structural cracking under frost heave deformation. These shortcomings limit their application in the harsh climate and complex geological conditions of alpine permafrost regions. The prefabricated corrugated steel plate retaining wall adopts a construction mode of factory-standardized prefabrication and on-site assembly, with the advantages of a high construction efficiency, a controllable construction period, no restriction from low-temperature seasons, and a strong flexible deformation capacity. It can effectively solve engineering challenges including tight construction schedules, insufficient structural frost heave resistance, and frequent post-construction defects. Significant comprehensive advantages are exhibited by this structure in terms of structural safety, durability, economy, energy conservation, and environmental protection, with broad application prospects in the field of transportation infrastructure construction in alpine permafrost regions.

Extensive research has been carried out by scholars on the engineering performance and application of corrugated steel plate structures, and abundant research results have been obtained. In terms of engineering applicability and economic benefits, the superior economic performance of corrugated plate structures compared with conventional masonry structures was verified through a comparative analysis by Ołdakowska et al. [1]. Multi-condition static load tests were carried out on a corrugated plate arch highway bridge after four years of service by Beben et al. [2], and the mechanical response characteristics of its long-term service were clarified. In terms of structural dynamic performance and seismic adaptability, the seismic response law of corrugated steel structures was studied by Davis et al. [3], and it was found that the deformation of the structure is dominated by section elliptization, which is significantly affected by the soil constraint, with a small structural inertia and good seismic adaptability. Hao et al. [4] investigates the temperature resistance of galvanized steel corrugated panel partitions in the inclined shafts of extra-long road tunnels. In terms of the soil–structure interaction mechanism, the displacement and bending moment distribution of corrugated steel plate structures were obtained via geodetic survey technology by Maleska et al. [5], and the controlling effect of soil characteristics on structural deformation was clarified. Based on the ABAQUS finite element model, the horizontal deformation law and structural stability of corrugated steel plate retaining walls under different load conditions were analyzed by Ji et al. [6], and the cooperative working mechanism between the fill and corrugated plates was revealed. In terms of numerical simulation methods and theoretical calculation, a novel homogenization model for the numerical modeling of corrugated steel plates was proposed by Pandit et al. [7], which realized the equivalent conversion of corrugated plates to planar isotropic plates, and the accuracy of the model was verified through static, buckling, and free vibration analyses. The structural moment of inertia was solved based on the waveform integration method by Xu et al. [8], and the differential equation model and theoretical calculation formula for the flexural deformation of corrugated steel retaining walls were derived, which provided theoretical support for the deformation analysis of flexible retaining structures. In addition, the superior stiffness and bearing capacity of corrugated

https://doi.org/10.3390/buildings16132532

steel plate shear walls compared with traditional flat plate structures were verified in relevant studies, which provided a reference for the optimization of mechanical properties of corrugated steel structures [9]. For the buckling performance of stiffened corrugated steel plate structures in alpine permafrost regions, the calculation formula for the buckling load was derived through finite element analysis and the Ritz method, and the correlation formula between the stiffener stiffness and buckling coefficient was proposed [10].

With the continuous expansion of the engineering construction scale in alpine permafrost regions, the mechanism of permafrost frost heave acting on retaining structures and corresponding prevention technologies have become a research hotspot in this research field. Existing studies have shown that the service performance of retaining structures in seasonally frozen ground and permafrost regions is significantly controlled by the frost heave effect. The frost heave depth and frost heave rate are the core parameters determining structural deformation, while multi-directional frost heave force, especially horizontal frost heave force, is the key inducement leading to the cracking, dislocation, and even overall instability of retaining structures [11]. In the field of the optimal design of retaining wall structures, a large number of systematic explorations have also been carried out. The multi-objective optimal design of reinforced concrete retaining wall structures was carried out by Das et al. [12], and the economically optimal scheme was achieved on the premise of meeting safety and stability requirements. The sensitivity of parameters such as backfill slope, foundation friction angle, and load conditions was analyzed by Kashani et al. [13], and a multi-objective optimization model balancing structural stability, total cost, and carbon emission was established. Intelligent optimization algorithms were adopted by Kayabekir et al. [14] and Öztürk et al. [15], respectively, to realize the multi-objective collaborative optimization of retaining wall structures integrating low carbon, economy, and safety—this design method for retaining walls was proposed. The sensitivity of structural parameters to the service performance of retaining structures was systematically analyzed by Saribas et al. [16], and a general idea and method for the optimal design of retaining walls were established.

In summary, the excellent engineering performance of corrugated steel plate structures has been clarified in existing studies [17–19], and extensive work has been carried out on the frost heave response of retaining structures in permafrost regions and the optimal design of retaining walls [20,21]. Nevertheless, three core research gaps still exist in current studies. First, most of the research on corrugated steel plate structures focus on conventional geological environments. Few studies pay attention to the structural response and environmental adaptability under the strong frost heave and large temperature difference in alpine permafrost regions. Second, the current research on permafrost retaining structures mainly focuses on traditional rigid structures. There is a lack of in-depth studies on the coordination mechanism between flexible corrugated steel plate retaining walls and permafrost. The mechanical property and deformation evolution law under frost heave conditions are also rarely discussed. Third, the existing optimization research on retaining walls does not fully consider the special environmental effects of highly cold permafrost, and systematic optimization research on key design parameters such as corrugation parameters, geometric dimensions, and tie reinforcement layout of corrugated steel plate retaining walls is seriously insufficient. Based on this, aiming at the structural performance and optimization problems of prefabricated corrugated steel plate retaining walls in alpine permafrost regions, the complex geological environment and harsh climatic conditions of alpine permafrost regions are fully considered in this paper. A thermo-mechanically coupled numerical model was established to investigate the structural behavior of the retaining wall system [22,23]. Based on previous research findings, this paper establishes a finite element model. The method combining finite element numerical simulation and an experimental test is adopted to systematically analyze the

influence law of key cross-sectional parameters including wall height, plate thickness, corrugation parameters (corrugation pitch, and corrugation height), and tie reinforcement layout on the deformation and internal force of corrugated steel plate retaining walls. Research on structural parameter optimization is carried out, the key controlling factors of structural performance are clarified, and the optimal parameter combination is proposed. The research results can provide a reliable theoretical basis for the design, construction, and long-term operation safety guarantee of corrugated steel plate retaining walls for highway engineering in alpine permafrost regions, with important engineering application value and broad popularization prospects.

2. Establishment and Validation of Finite Element Model

2.1. Project Overview

The project considered in this study is located in western China. Affected by the North Tianshan and South Tianshan Mountain Systems, the climate in this region presents certain warm and humid characteristics, along with the distinct attributes of a continental arid and semi-arid climate. Under extreme climatic conditions, the local maximum temperature reaches 38.5 °C, and the minimum temperature drops to −37.4 °C. The maximum observed snow depth over the years is approximately 30 to 40 cm, and the maximum seasonal frozen ground depth in the urban area is about 92 cm. In accordance with the Code [24], the seasonal frozen ground depth in the project area ranges from 0.92 m to 2.0 m, and it is recommended that the foundation embedment depth be set below the seasonal frozen ground depth. In a seasonally frozen ground environment, the soil undergoes an ice–water phase transformation as the ambient temperature fluctuates, leading to significant differences in its engineering properties. When the ground temperature decreases to meet the freezing condition, soil expansion is induced, as the specific gravity of ice is lower than that of water, and ice of the same mass occupies a larger volume. When the temperature rises, the ice originally existing in the soil gradually melts into water, the compactness of the soil structure decreases accordingly, and shrinkage occurs, which finally manifests as surface subsidence or collapse. In this frozen ground distribution area, natural slopes, highway and railway subgrade slopes, retaining walls, and foundation engineering are universally affected by freeze–thaw cycles, which are prone to triggering engineering damage and posing potential threats to national economic construction and operational safety.

2.2. Establishment of the Finite Element Model (FEM)

The finite element model was established using ANSYS 2021R1 software, a widely used platform for structural mechanics and multi-physics coupling analysis in civil engineering. This software provides robust element libraries and solution capabilities suitable for simulating soil–structure interaction and temperature field effects in retaining wall systems.

2.2.1. Dimensional Parameters of the Corrugated Steel Plate Retaining Wall

A corrugated steel plate retaining wall with a height of 3.0 m, a longitudinal length of 10.8 m, and a backfill width behind the wall of 12.8 m was selected for this study. The thickness of the corrugated steel plate was set to 6.0 mm, the section size of the concrete foundation was 0.8 m × 0.8 m, the laying length of the tie reinforcement strips was 10.0 m, the horizontal spacing of the tie reinforcements was 1.2 m, and the vertical row spacing was 1.0 m. The specific modeling steps are as follows:

(1) The half corrugation curve was drawn with corrugation parameters of corrugation pitch × corrugation height (400 mm × 150 mm), and the thickness of the corrugated

steel plate was set to 6 mm. Corrugations of the required length were generated through mirroring and copying, and merged via Boolean operation. Finally, the retaining wall model was established by linear extrusion, as shown in Figure 1a.

(2) The soil mass model was created, and the cutting treatment between the soil mass and the retaining wall was performed through a Boolean operation to obtain the final soil mass model, as shown in Figure 1b.

(3) The Boolean operation was applied again to cut the concrete foundation model from the soil mass model. The tie reinforcement model was generated by cutting the soil mass with the corresponding geometric features. The meshed finite element model is shown in Figure 1c,d.

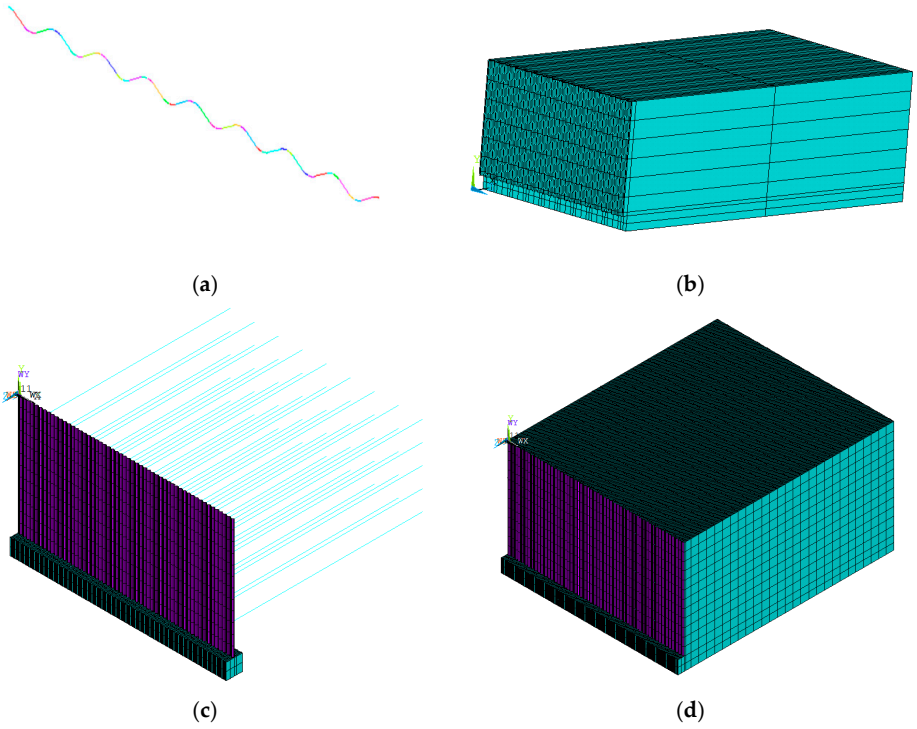

Figure 1. Establishment of the finite element model: (**a**) creation of corrugation curves; (**b**) soil; (**c**) corrugated steel plate retaining wall; and (**d**) model of retaining wall and backfill structure behind the wall.

2.2.2. Selection of Element Types

SHELL181 shell elements are adopted for the corrugated steel plate. As the main load-bearing component of the retaining wall, the corrugated steel plate is subjected primarily to bending and shear forces, making shell elements suitable for the numerical modeling. It is a four-node elastic thin-shell element with six degrees of freedom per node, capable of simulating the bending, shear, and axial deformation behaviors of thin-walled structures accurately. SHELL181 supports large-deformation analysis and geometric nonlinearity, and is suitable for characterizing the structural behavior of corrugated steel plates, especially in high-stress regions and under local deformation conditions, where relatively accurate results can be obtained. In addition, SHELL131 elements are used for the corrugated steel plate in the temperature field analysis. As a thermal shell element, it can account for heat conduction effects both in-plane and through the thickness direction, and is therefore applicable to temperature field calculations of thin-walled structures.

The governing equations for transient heat transfer are given as follows:

$$\rho c \frac{\partial T}{\partial t} = \frac{\partial}{\partial x}\left(k_x \frac{\partial T}{\partial x}\right) + \frac{\partial}{\partial y}\left(k_y \frac{\partial T}{\partial y}\right) + \frac{\partial}{\partial z}\left(k_z \frac{\partial T}{\partial z}\right) + Q \quad (1)$$

where ρ is the density, c is the specific heat capacity, k is the thermal conductivity, T is the temperature, t is the time, and Q is the internal heat generation.

The structural equilibrium equation is as follows:

$$\sigma_{ij,j} + \rho b_i = \rho \ddot{u}_i \quad (2)$$

where $\sigma_{ij,j}$ is the stress tensor, b_i is the body force vector, and u_i is the displacement vector.

The thermal-stress coupling equation is as follows:

$$\sigma_{ij} = D_{ijkl}\varepsilon_{kl} - D_{ijkl}\alpha_{kl}\Delta T \quad (3)$$

where D_{ijkl} is the elasticity tensor, ε_{kl} is the total strain tensor, α_{kl} is the thermal expansion coefficient tensor, and ΔT is the temperature change.

The thermal field and structural field are linked within the finite element framework. The specific steps are as follows: (1) An initial steady-state temperature field is first established using the long-term average ground temperature conditions. (2) A transient thermal analysis is subsequently performed using the annual atmospheric temperature boundary conditions to obtain the temporal and spatial temperature distribution within the retaining wall–soil system. (3) The temperature results obtained at each time step are transferred to the structural analysis module as thermal body loads. (4) Frost-heave strain induced by temperature variation is introduced through the frost-heave constitutive formulation. (5) Thermal strain, frost-heave strain, earth pressure, and self-weight are then simultaneously considered in the structural analysis to calculate the displacement and stress responses. (6) Finally, the structural responses throughout the freeze–thaw cycle are extracted and analyzed.

In the structural analysis stage, the temperature field is applied to the structural model as a load, thereby realizing the coupled analysis of the temperature field and the structural field. SOLID185 elements are used for the concrete foundation and the backfill structure behind the wall. BEAM188 beam elements are adopted to model the reinforcement strips in the corrugated steel plate retaining wall. The contact between the corrugated steel plate and the soil mass, as well as the interaction between the concrete foundation and the soil mass, are simulated using CONTA174 contact elements and TARGE170 target elements. The contact behavior between the corrugated steel plate, concrete foundation, and backfill soil is simulated by pairing CONTA174 contact elements with TARGE170 target elements. The key contact parameters are defined with a clear basis: (1) The interface friction coefficient between the corrugated steel and gravel backfill is determined by laboratory direct shear tests, with a calibrated value of 0.4, which conforms to the interface mechanical characteristics of the Q235 steel and graded gravel filler used in the field test section. (2) The normal contact stiffness, tangential contact stiffness, and penetration tolerance adopt the recommended default settings of ANSYS program, which have been widely verified and validated in previous soil–structure interaction numerical simulations of retaining walls. (3) The contact algorithm adopts the augmented Lagrange method, and the initial contact state is set as closed bonding contact. All contact parameter settings are further calibrated and verified by field measured displacement and earth pressure data, which eliminates the numerical divergence caused by unreasonable contact parameter assignment and ensures the accuracy of the soil–structure interaction simulation.

2.2.3. Material Parameters and Constitutive Models

The mechanical parameters of the corrugated steel plate are set with reference to the experimental data and in combination with the local topographical, geological, and hydrological conditions. The model mainly involves the definition of four material properties, namely, the corrugated steel plate, concrete foundation, reinforcement strips, and backfill behind the wall. The specific material parameters are presented in Tables 1 and 2.

Table 1. Material parameters of the retaining wall.

Material Type	Weight	Elastic Modulus	Poisson's Ratio	Cohesion	Internal Friction Angle	Thermal Conductivity λ	Specific Heat Capacity c
Unit	kN/m³	MPa	--	kPa	°	W/(m·°C)	J/(kg·°C)
Corrugated Steel Plate	78.5	2.06×10^5	0.3	--	--	52	460
Concrete Foundation	24	3.0×10^4	0.25	--	--	2.	900
Backfill Behind the Wall	20	28	0.32	20	35°	1.5	1800

Table 2. Parameters of steel–plastic reinforcement strips.

Material	Specification	Horizontal Spacing	Vertical Spacing	Breaking Tensile Force	Apparent Friction Coefficient	Unit Weight	Thermal Conductivity λ
Unit	mm	mm	mm	kN	--	g/m	W/(m·°C)
CAT30020B	30 × 2	600	700	9	0.4	91	0.4

When carbon structural steel is selected for the corrugated steel plate, Grade Q235 steel is generally recommended. When high-strength low-alloy structural steel is adopted, Grade Q355 is the preferred option. For engineering conditions in corrosive environments or with high requirements for durability, weathering structural steel shall be preferentially used as the material of the corrugated steel face plate, and Grade Q235NH or Q355NH steel is generally applicable. The mechanical properties of the steel plate shall comply with the provisions in the table below, and other technical indicators shall meet the relevant requirements of the following national standards [25–27]. The mechanical properties of the corrugated steel plate are presented in Table 3.

Table 3. Mechanical properties of corrugated steel plates.

Material Name	Steel Grade	Yield Strength/MPa	Tensile Strength/MPa	Elongation After Fracture/%
Carbon Structural Steel	Q235	≥235	≥370	≥26
High-Strength Low-Alloy Steel	Q355	≥355	≥470	Horizontal ≥ 20, longitudinal ≥ 22
Weathering Structural Steel	Q 235NH	≥235	≥360	≥25
	Q 355NH	≥355	≥490	≥22

The corrugation profile (corrugation parameters), geometric dimensions, and allowable deviations of the corrugated steel face plate shall comply with the provisions in Table 4.

Table 4. Geometric parameters of corrugated steel plates.

	Item	Specified Dimension/mm	Allowable Deviation
Corrugation Profile (Corrugation Parameters)	Corrugation Pitch l	400	±3 mm
	Corrugation Height d	150	±3 mm
	Arc Radius at Crest or Trough	80	±2 mm
Geometric Dimensions	Wall Thickness t	6	Not less than the design value
	Standard Single Plate Length LC	3000	±1%
	Standard Single Plate Width LW	1280	±1%

The volume strain due to frost heave is calculated as follows:

$$\varepsilon_{fv} = \alpha_f \theta_u \frac{\partial T}{\partial z} \Delta t \quad (4)$$

where a_f is the frost heave coefficient, θ_u is the unfrozen water content, and $\frac{\partial T}{\partial z}$ is the vertical temperature gradient.

All model parameters were obtained from laboratory tests on soil samples collected from the project site. The initial steady-state temperature field based on the average annual temperature was calculated. The 12-month transient thermal analysis with a time step of 1 day to obtain the temperature distribution at each time step was performed. Furthermore, the temperature field results were imported into the structural analysis module as body loads to calculate the thermal stress and deformation. The Drucker–Prager plasticity model was adopted to simulate the nonlinear behavior of the soil, which is widely accepted for geotechnical engineering problems involving pressure-dependent materials. The yield function is defined as follows:

$$F = \alpha I_1 + \sqrt{J_2} - k = 0 \quad (5)$$

where I_1 is the first invariant of the stress tensor, J_2 is the second invariant of the deviatoric stress tensor, and a and k are the material constants related to the friction angle ϕ and cohesion c.

An associated flow rule was adopted, whereby the plastic potential function is identical to the yield function. The soil was assumed to behave elastically below the yield stress and plastically once the yield stress is exceeded. The Coulomb friction model is used to simulate the interaction between the corrugated steel plate and the backfill soil. The interface friction angle was set to two-thirds of the soil internal friction angle ($\delta = 21^\circ$), which is a commonly accepted value for steel–soil interfaces. Both tangential friction and normal contact behavior were considered, with separation allowed when the normal stress becomes tensile. A sensitivity analysis was performed, showing that the interface friction angle has a relatively small effect (less than 8%) on the overall structural response within the typical range of values.

2.2.4. Boundary Conditions and Mesh Generation

During the numerical simulation of the retaining wall, the constraint conditions mainly involve the control of structural displacement, and the boundary conditions are set as follows: Full constraint is applied to the bottom surface of the model. Horizontal constraints are imposed on both ends of the foundation and one end of the backfill behind the wall, which only limit the displacement in the horizontal direction while allowing free deformation in the vertical direction. Constraints in the X direction are applied to the boundaries of the front and rear retaining walls of the model and the connected soil mass, which only restrict the displacement along the X direction, while the displacements in the vertical direction and the other horizontal direction remain free. The top surface of the

backfill is set as a free surface, which can deform freely with the stress of the structure. Alpine permafrost regions are characterized by typical features such as long and cold winters, short summers, large diurnal temperature differences, and intense solar radiation. The surface temperature presents significant periodic changes, and is notably affected by wind speed and radiation. Due to the difference in the thermal conductivity of constituent materials, the temperature field distribution of the prefabricated corrugated steel plate retaining wall shows significant inhomogeneity. Therefore, in the numerical simulation, the boundary conditions of the temperature field shall be reasonably set in combination with the regional climatic characteristics.

Based on 30-year meteorological records from the project site, we used a sinusoidal function to represent the annual temperature variation:

$$T(t) = T_{avg} + T_{amp} \sin(\frac{2\pi}{365}(t - t_0)) \quad (6)$$

where T_{avg} = −2.3 °C, T_{amp} = 18.7 °C, and t_0 = 196 (the day of the year with the maximum temperature).

The measured ground temperature data at different depths were used to define the lower boundary condition and the insulation effect of the backfill soil and the steel plate surface was considered.

In addition, the quality of mesh generation has a direct impact on the accuracy of the analysis results and computational speed, which is a non-negligible key link in the entire analysis process. The mapped mesh generation method is adopted for the model in this study. The mapped mesh requires relatively regular geometric shapes and is applicable to the generation of regular element types, including triangular, quadrilateral, tetrahedral, pentahedral, and hexahedral elements. Elements generated by this method are of favorable quality, which can effectively improve the accuracy and stability of the solution. Quadrilateral elements are selected for the corrugated steel plate, and hexahedral solid elements are adopted for the backfill behind the corrugated plate retaining wall. For the corrugated steel plate retaining wall, mesh generation shall be carried out first for the reinforcement strips, followed by the corrugated steel plate, and, finally, for the surrounding soil mass. A grid convergence study was conducted with three different grid densities: coarse (12,456 elements), medium (28,734 elements), and fine (56,218 elements). It was shown by the results that the difference in maximum displacement between the medium and fine grids is less than 2.3%, indicating that the medium grid density is sufficient for accurate calculations.

2.3. Experimental Validation

Figure 2 shows the experimental test setup of the corrugated steel plate retaining wall. An experimental test section was selected to design and implement experimental test research on the corrugated steel plate retaining wall. The mechanical and deformation laws of the structure throughout the construction process were analyzed and compared with the numerical simulation results, to comprehensively evaluate the accuracy of the model in simulating the deformation law and force transfer path of the corrugated plate retaining wall.

Figure 3 presents the displacement and stress curves derived from the test and simulation data. Three monitoring sections along the length of the retaining wall (Section A–A at 10 m, Section B–B at 30 m, and Section C–C at 50 m) were included in our field test. It can be seen from the figure that the FEM can accurately reflect the overall deformation characteristics of the corrugated steel plate retaining wall under earth pressure. The simulation results are in good agreement with the test results in terms of the variation trend and distribution law of the horizontal displacement of the wall. The variation of wall displacement with height presents a typical deformation mode of retaining walls. Both the test and simulation results show that the horizontal displacement increases with the rise in wall height, reaches the peak at the wall top (3 m height), and approaches 0 at the wall

bottom (0 m height). This accurately reproduces the typical flexural deformation characteristics of the corrugated steel retaining wall as a vertical cantilever member under dynamic load. The comparative stress analysis results show that the finite element model can reasonably simulate the stress state of the corrugated steel plate retaining wall. Both the test and simulation results present the distribution characteristics that the stress increases with the decrease in wall height, reaches the peak at the wall bottom, and approaches 0 at the wall top. This accurately reflects the core mechanical characteristics of cantilever retaining walls under a lateral dynamic load: the bending moment increases downward along the wall height, and the wall bottom section is the most unfavorable stress-bearing section. The simulated stress curve fits well with the measured test curve within the full height range. The slight fluctuation of the FEM curves is attributed to the refined mesh at corrugation crests and troughs, which captures local stress concentration and micro-deformation characteristics. In contrast, the field test data reflect the average measured response of discrete sensors over a certain area, resulting in smoother curves. The overall trend and peak values of the simulation and test results are in good agreement, verifying the reliability of the finite element model. Based on the comprehensive comparison results of displacement and stress, the FEM of the corrugated steel plate retaining wall established in this paper can accurately reflect the deformation characteristics and mechanical laws of the structure under test conditions, which can be used as an effective numerical analysis tool for subsequent research on structural parameter analysis and the optimal design of corrugated steel plate retaining walls.

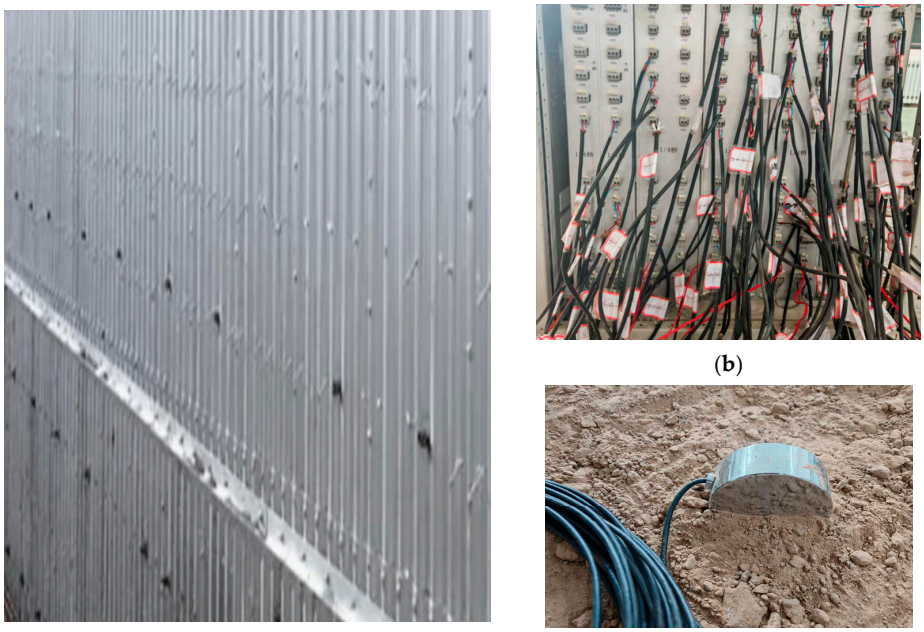

(**a**) (**b**) (**c**)

Figure 2. Experimental test of corrugated steel plate retaining wall: (**a**) experimental test site; (**b**) data acquisition equipment; and (**c**) earth pressure sensor.

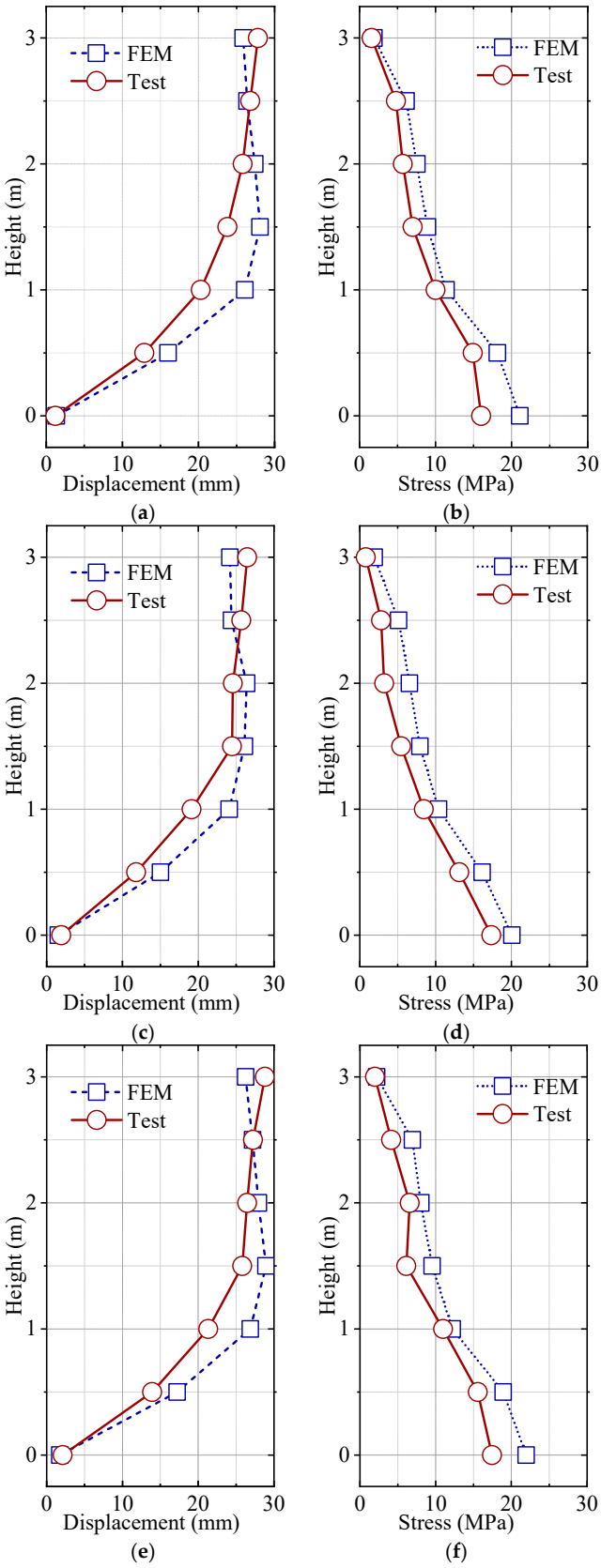

Figure 3. Comparison of dynamic response of corrugated steel plate retaining wall between test and numerical simulation: (**a**) horizontal displacement of Section A–A at 10 m; (**b**) stress of Section A–A

at 10 m; (**c**) horizontal displacement of Section B–B at 30 m; (**d**) stress of Section B–B at 30 m; (**e**) horizontal displacement of Section C–C at 50 m; and (**f**) stress of Section C–C at 50 m.

3. Influence of Section Form on Mechanical Performance of Corrugated Steel Plate Retaining Wall

Using the validated finite element model in Section 2, the influence laws of key parameters of the corrugated steel plate retaining wall on its mechanical performance and deformation characteristics are systematically analyzed. A parametric analysis is carried out focusing on factors such as the corrugation parameters of the steel plate, wall height, plate thickness, and layout of tie reinforcements, to explore the variation characteristics of the displacement response, stress distribution, and overall stability of the retaining wall under different parameter combinations.

3.1. Influence of Wall Heights on the Mechanical Performance of Corrugated Steel Plate Retaining Walls

Five conditions with wall heights of 2 m, 4 m, 6 m, 8 m, and 10 m are selected, respectively, to analyze the influence of retaining walls with different heights on the horizontal displacement of the corrugated steel plate and the equivalent stress of the retaining wall under the action of self-weight and lateral earth pressure. By analyzing the deformation and stress results, the mechanical and deformation laws of the corrugated plate retaining wall under different heights are obtained. Except for the wall height parameter, all other geometric dimensions, material parameters, boundary conditions, and load conditions are kept consistent to ensure the comparability of the analysis results.

3.1.1. Horizontal Displacements of Corrugated Steel Plate Retaining Walls

Figure 4 shows the horizontal displacement of corrugated steel plate retaining walls with different heights under the corresponding conditions, considering the retaining wall weight and the backfill behind the wall back. It can be seen from the figure that, under the action of self-weight and lateral earth pressure, the horizontal displacement trends of the corrugated steel plate walls with different heights are basically consistent, all presenting a bulging phenomenon characterized by an outward protrusion in the middle and lower parts and a contraction in the upper part. For retaining wall heights of 2 m, 4 m, 6 m, 8 m, and 10 m, the corresponding maximum horizontal displacements of the corrugated steel plate wall are 14.17 mm, 37.08 mm, 58.43 mm, 109.40 mm, and 162.91 mm, respectively. The horizontal displacement of the corrugated steel plate wall increases gradually with the wall height rising from 2 m to 10 m, showing a nonlinear growth trend.

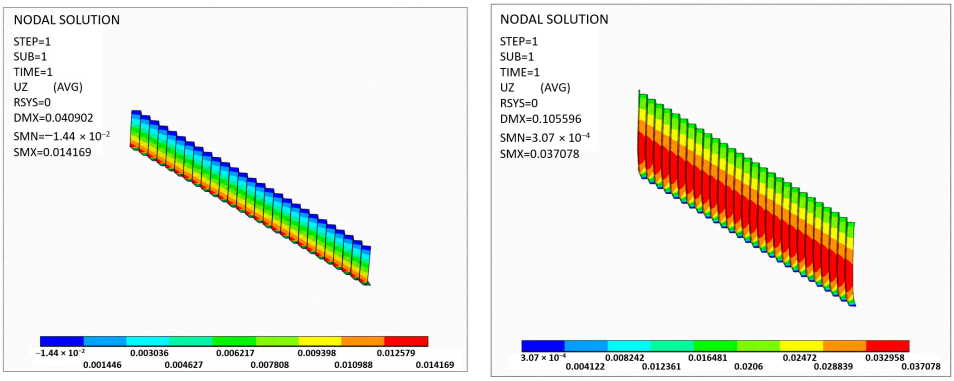

(**a**) (**b**)

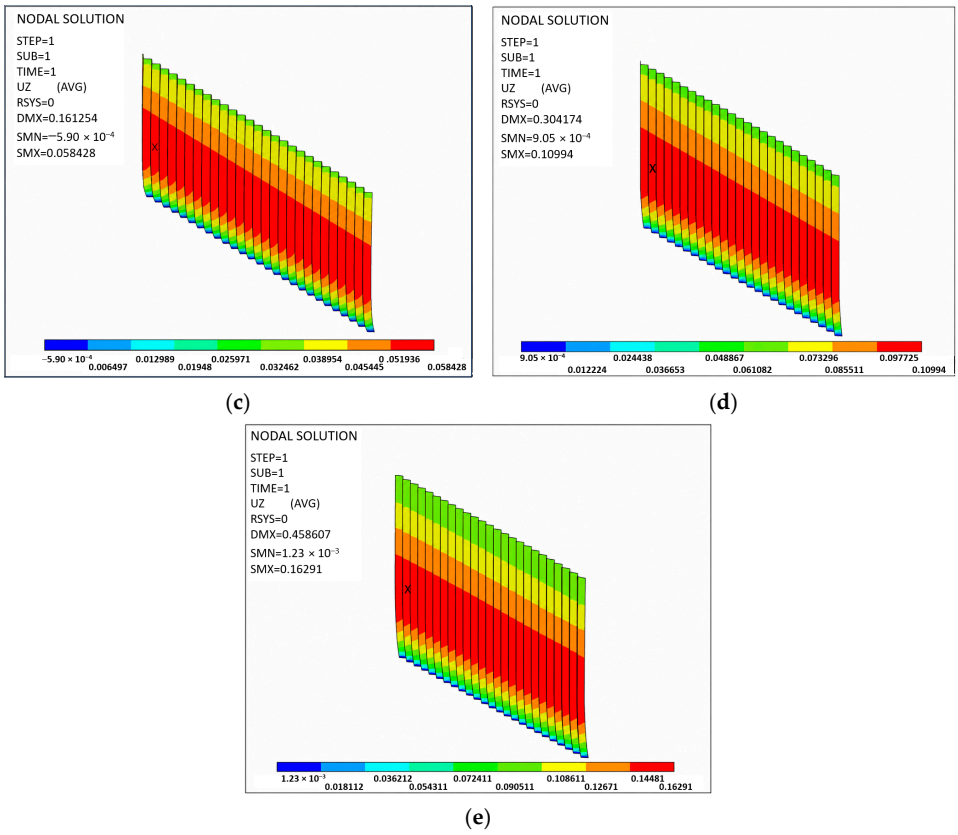

Figure 4. Contour plots of horizontal displacement of corrugated steel plate retaining walls with different heights: (**a**) wall height 2 m; (**b**) wall height 4 m; (**c**) wall height 6 m; (**d**) wall height 8 m; and (**e**) wall height 10 m.

Figure 5 presents the distribution curves of horizontal displacement along the wall height of the corrugated steel plate retaining wall under different wall height conditions. As the wall height increases to 6 m, the horizontal displacement of the wall rises significantly, the displacement curve begins to concentrate in the middle and upper parts of the wall, and the retaining wall gradually exhibits the characteristics of a flexible structure. When the wall height further increases to 8 m and 10 m, the horizontal displacement of the wall is dramatically amplified, the maximum displacement value multiplies compared with that under low wall height conditions, and the position of the maximum displacement obviously shifts to the middle and upper areas of the wall. The nonlinear increase in displacement and stress when wall height exceeds 6 m is due to the transition from "flexural-dominated" to "shear–flexural-dominated" behavior. For walls below 6 m, the structural response is mainly controlled by bending deformation. For walls above 6 m, shear deformation becomes significant, leading to a faster increase in displacement and stress.

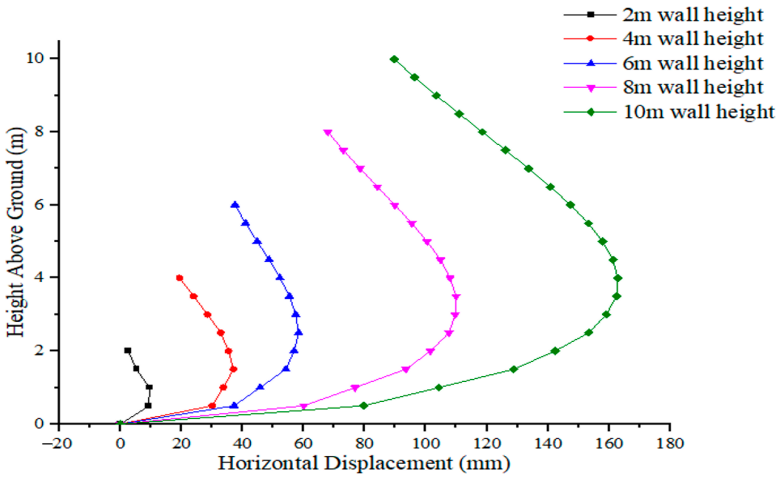

Figure 5. Horizontal displacement curves of corrugated steel plate retaining walls with different heights.

3.1.2. Stress of Corrugated Steel Plate Retaining Walls

Figure 6 presents the equivalent stress for corrugated steel plate retaining walls under conditions with different wall heights. As shown in the figure, under the action of self-weight and lateral earth pressure, the equivalent stress trends of corrugated steel plate retaining walls with different heights are basically consistent. All walls exhibit the distribution characteristic of low stress in the upper section and high stress in the lower section, with the maximum stress occurring at the junction between the corrugated steel plate and the concrete foundation. The maximum equivalent stress of the corrugated steel plate wall is approximately 10.9 MPa at a retaining wall height of 2 m, and increases to 32.1 MPa, 57.6 MPa, 86.3 MPa, and 118 MPa for wall heights of 4 m, 6 m, 8 m, and 10 m, respectively. The equivalent stress of the corrugated plate wall rises gradually with the increase in the retaining wall height.

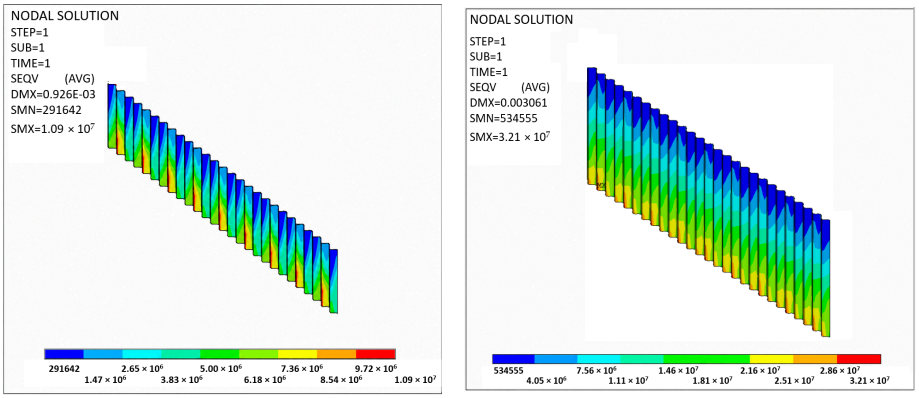

(**a**) (**b**)

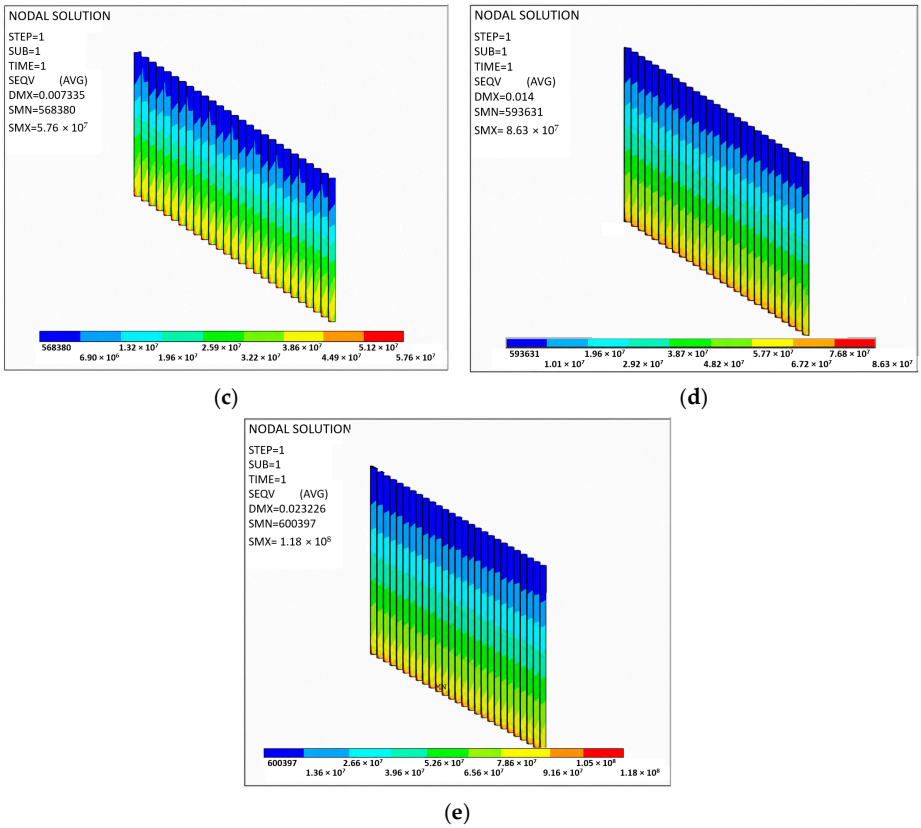

Figure 6. Contour plots of equivalent stress of corrugated steel plate retaining walls with different heights: (**a**) wall height 2 m; (**b**) wall height 4 m; (**c**) wall height 6 m; (**d**) wall height 8 m; and (**e**) wall height 10 m.

Figure 7 presents the distribution of equivalent stress along the wall height of the corrugated steel plate retaining wall under different wall height conditions. As can be seen from the figure, with the increase in wall height, the equivalent stress level of the corrugated steel plate increases significantly. For retaining walls with low heights (2 m and 4 m), the overall equivalent stress of the wall is low, and the stress state is relatively safe. As the wall height increases to 6 m, the stress in the bottom and middle–lower regions of the wall rises significantly, and the phenomenon of stress concentration begins to appear. When the wall height further increases to 8 m and 10 m, the equivalent stress at the bottom of the wall increases dramatically, the range of the high-stress zone expands significantly, and the stress state of the structure tends to be unfavorable. In terms of the stress distribution pattern, the gradient of stress along the wall height increases gradually with the rise of wall height. When the wall height exceeds 6 m, the bending effect borne by the middle–lower region of the corrugated steel plate becomes more significant, indicating that the increase of wall height not only raises the peak stress, but also aggravates the stress inhomogeneity within the structure. Therefore, the wall height is one of the key parameters affecting the mechanical performance of corrugated steel plate retaining walls. When the wall height exceeds 6 m, the stress level in the bottom and middle–lower regions of the wall increases significantly. If the structure is not strengthened by measures such as increasing the thickness of the corrugated steel plate, optimizing the corrugation parameters, or strengthening the layout of tie reinforcements, an unfavorable stress state is prone to occur. Therefore, for high-wall engineering in alpine permafrost regions, the wall height shall be taken as a key control parameter for structural design and optimization.

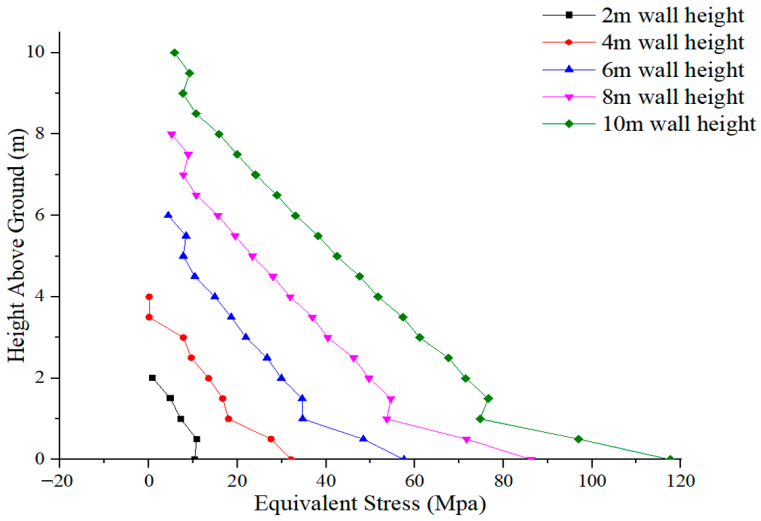

Figure 7. Equivalent stress curves of corrugated steel plate retaining walls with different heights.

3.2. Influence of Plate Thicknesses on the Mechanical Performance of Corrugated Steel Plate Retaining Walls

In Section 3.1, the displacement characteristics and stress distribution patterns of corrugated steel plate retaining walls under different wall height conditions are systematically investigated, and the adverse effects of increasing wall height on the overall structural stability and safety are clarified. However, in practical engineering, the wall height is often limited by topographical conditions and functional requirements, so it is difficult to achieve the effective control of the structural performance through a single adjustment. The analysis shows that, when the wall height is 6 m, the retaining wall presents obvious mechanical characteristics in terms of displacement, stress, and soil deformation, which can fully reflect the mechanical and deformation laws of the structure and has strong engineering representativeness. Therefore, the wall height of 6 m is selected as the typical research condition in this paper. On the premise of keeping other parameters unchanged, only the thickness of the corrugated steel plate is changed, to systematically analyze the influence law of plate thickness variation on the horizontal displacement, stress distribution, and overall stability of the retaining wall.

3.2.1. Horizontal Displacements of Corrugated Steel Plate Retaining Walls

Figure 8 presents the horizontal displacement of corrugated steel plate walls with different plate thicknesses under conditions with plate thicknesses of 4 mm, 5 mm, 6 mm, 7 mm, 8 mm, and 9 mm. As shown in the figure, under the action of self-weight and lateral earth pressure, the horizontal displacement patterns under different plate thicknesses exhibit similar overall characteristics, all presenting a bulging phenomenon characterized by an outward protrusion in the middle and lower parts and a contraction in the upper part. The horizontal displacement of the corrugated steel plate retaining wall is approximately 106.68 mm at a plate thickness of 4 mm, and decreases to 71.33 mm, 58.43 mm, 53.57 mm, 49.47 mm, and 45.95 mm for plate thicknesses of 5 mm, 6 mm, 7 mm, 8 mm, and 9 mm, respectively. The horizontal displacement of the corrugated steel plate wall decreases gradually as the plate thickness increases from 4 mm to 9 mm. As the plate thickness increases from 4 mm to 9 mm, the horizontal displacement of the retaining wall continuously decreases, but the reduction rate gradually declines. Specifically, the displacement decreases by 33.13% when the thickness increases from 4 mm to 5 mm, and further decreases by 18.08% when increased to 6 mm. Thereafter, each additional 1 mm increment in thickness yields reductions of 8.32%, 7.65%, and 7.11%, respectively,

indicating that the marginal benefit of increasing plate thickness for displacement control diminishes significantly once the thickness exceeds 6 mm.

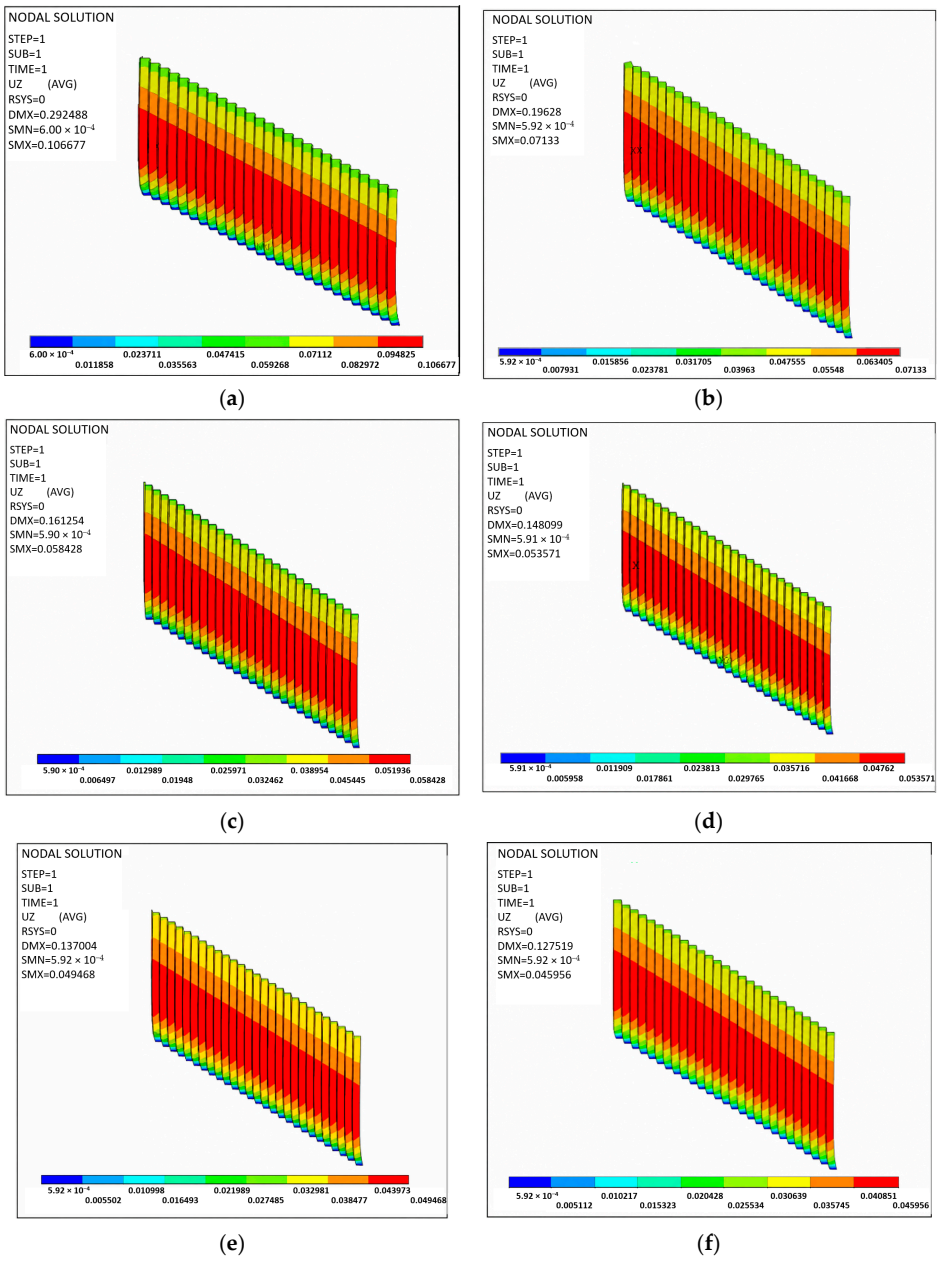

Figure 8. Horizontal displacement contour plots of corrugated steel plate retaining walls with different plate thicknesses: (**a**) plate thickness 4 mm; (**b**) plate thickness 5 mm; (**c**) plate thickness 6 mm; (**d**) plate thickness 7 mm; (**e**) plate thickness 8 mm; and (**f**) plate thickness 9 mm.

Figure 9 presents the distribution curves of horizontal displacement along the wall height of the corrugated steel plate retaining wall under different plate thickness conditions. It can be seen from the figure that the overall horizontal displacement of the retaining wall shows a significant decreasing trend with the gradual increase in the plate thickness of the corrugated steel plate. The largest horizontal displacement occurs when the plate thickness is 4 mm, with the displacement curve shifting outward. When the plate thickness increases to 5 mm and 6 mm, the horizontal displacement of the wall decreases

significantly, indicating that increasing the plate thickness can effectively improve the overall stiffness of the structure and enhance its resistance to lateral earth pressure.

Under different plate thickness conditions, the distribution pattern of horizontal displacement of the retaining wall along the height direction is basically consistent, all presenting the characteristic of a "small displacement at the bottom and large displacement at the middle and upper parts", and the maximum horizontal displacement usually occurs in the middle and upper areas of the wall. This indicates that the change in plate thickness does not alter the basic deformation mode of the wall, but mainly affects the magnitude of displacement. When the plate thickness increases from 4 mm to 6 mm, the displacement curve moves inward significantly, with a remarkable reduction in the maximum horizontal displacement. As the plate thickness further increases to 7 mm, 8 mm, and 9 mm, the displacement continues to decrease, but the spacing between the curves gradually narrows, indicating that the effect of a plate thickness increase on displacement control begins to weaken in the range of 7 mm to 9 mm. When the plate thickness is 6 mm, the maximum horizontal displacement of the retaining wall decreases significantly and is basically controlled within the engineering reference range of 60 mm, which can well meet the deformation requirements under the serviceability limit state. When the plate thickness further increases to 7 mm and above, the maximum horizontal displacement of the wall is further reduced, but the reduction rate is not significant compared with that under the 6 mm plate thickness condition. The diminishing improvement effect with increasing plate thickness is because the structural stiffness is not only determined by the plate thickness but also by the tie reinforcement. Beyond a critical thickness, increasing the plate thickness does not significantly increase the overall system stiffness.

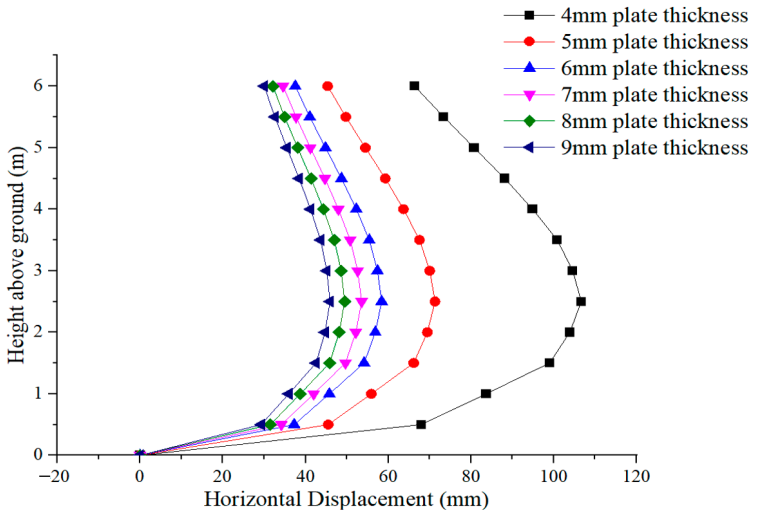

Figure 9. Horizontal displacement curves of corrugated steel plate walls with different plate thicknesses.

3.2.2. Stress of Corrugated Steel Plate Retaining Walls

Figure 10 presents the equivalent stress for corrugated steel plate retaining walls with a height of 6.0 m under conditions with plate thicknesses of 4 mm, 5 mm, 6 mm, 7 mm, 8 mm, and 9 mm. As shown in the figure, under the action of self-weight and lateral earth pressure, the equivalent stress trends of corrugated steel plate retaining walls with different plate thicknesses are basically consistent. All walls exhibit the distribution characteristic of low stress in the upper section and high stress in the lower section, with the maximum stress occurring at the junction between the corrugated steel plate and the concrete foundation. The equivalent stress of the corrugated steel plate retaining wall is

approximately 74.0 MPa at a plate thickness of 4 mm, and decreases to 64.6 MPa, 57.6 MPa, 52.0 MPa, 47.6 MPa, and 43.8 MPa for plate thicknesses of 5 mm, 6 mm, 7 mm, 8 mm, and 9 mm, respectively. The equivalent stress of the corrugated steel plate wall decreases gradually as the plate thickness increases from 4 mm to 9 mm.

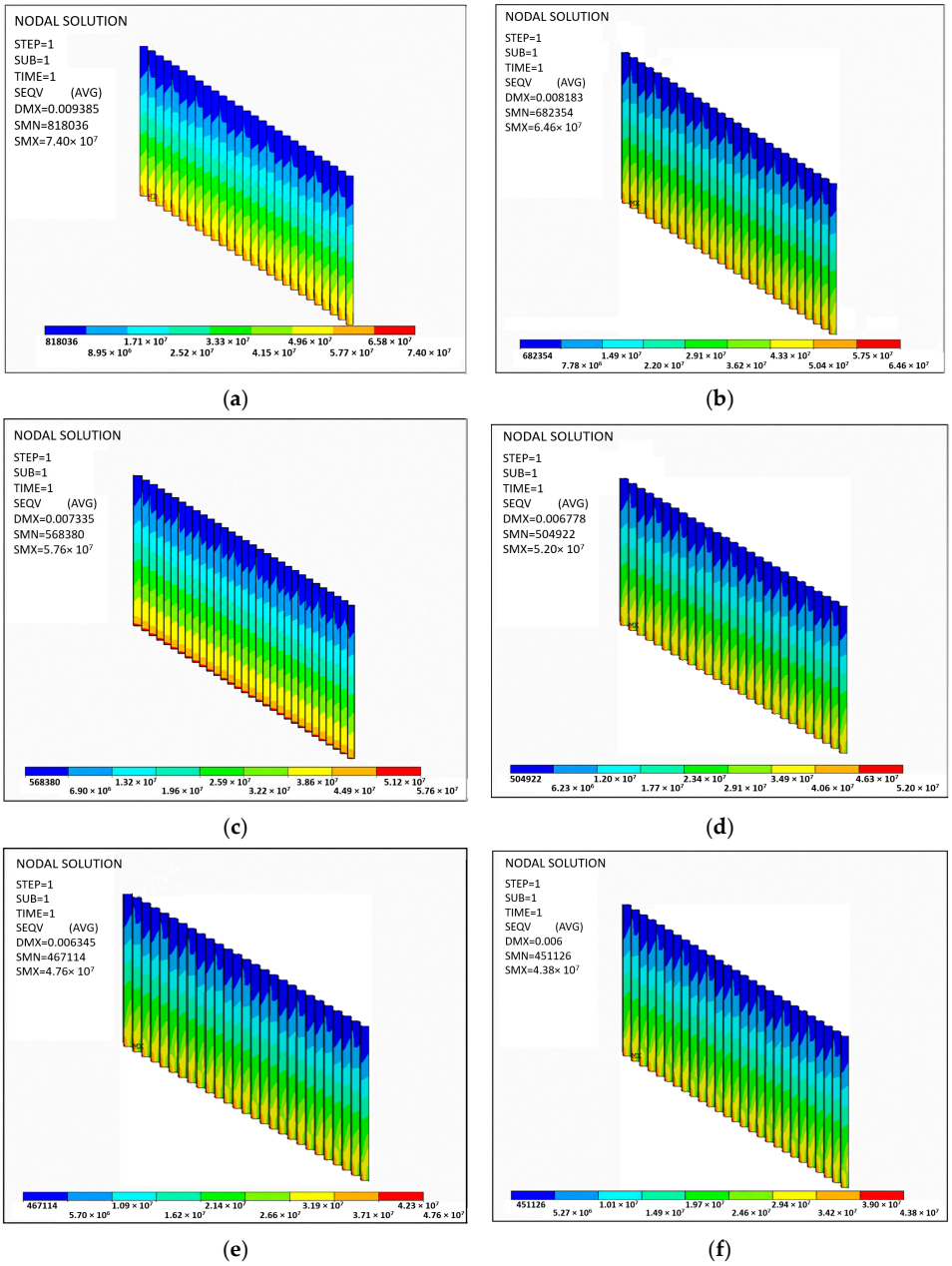

Figure 10. Equivalent stress contour plots of corrugated steel plate retaining walls with different plate thicknesses: (**a**) plate thickness 4 mm; (**b**) plate thickness 5 mm; (**c**) plate thickness 6 mm; (**d**) plate thickness 7 mm; (**e**) plate thickness 8 mm; and (**f**) plate thickness 9 mm.

Figure 11 shows the equivalent stress distribution along the wall height under different corrugated steel plate thicknesses (4 mm to 9 mm) at a wall height of 6 m. It can be seen from the figure that as the plate thickness gradually increases, the overall equivalent stress level of the retaining wall shows a significant decreasing trend. The equivalent stress is the largest at a plate thickness of 4 mm, especially in the middle and lower parts of the wall where the stress level is relatively high. When the plate thickness increases to

5 mm and 6 mm, the stress value decreases significantly, indicating that increasing the plate thickness can effectively improve the bending stiffness and bearing capacity of the corrugated steel plate, thereby reducing the internal force response of the structure. Under different plate thickness conditions, the stress distribution pattern of the corrugated steel plate is basically consistent: high-stress regions are mainly concentrated at the bottom and middle–lower parts of the wall, and gradually decrease along the wall height. This indicates that the change in plate thickness does not alter the main stress mode of the retaining wall, but mainly adjusts the magnitude of the stress. As the plate thickness increases from 4 mm to 6 mm, the stress curve shifts significantly to the left, and the range in the high-stress zone is obviously reduced. When the plate thickness further increases to 7 mm, 8 mm, and 9 mm, the stress level continues to decrease, but the spacing between different curves gradually narrows, showing the characteristic of a diminishing marginal effect of the plate thickness on stress control.

Based on the comparison of the maximum equivalent stress under various conditions, there is an obvious nonlinear negative correlation between the corrugated steel plate thickness and the maximum equivalent stress. In the range of small plate thicknesses, increasing the plate thickness can significantly reduce the maximum equivalent stress. However, when the plate thickness reaches a certain level, the improvement effect of further increasing the plate thickness on the stress level tends to be limited.

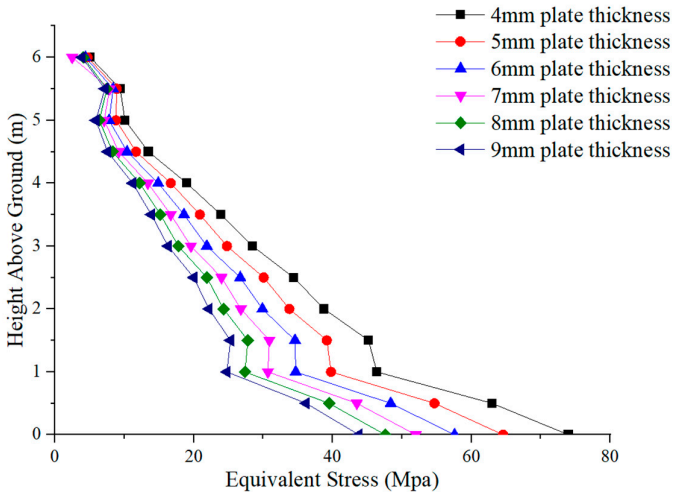

Figure 11. Equivalent stress curves of corrugated steel plate retaining walls with different plate thicknesses.

3.3. Influence of Corrugation Profiles on the Mechanical Performance of Corrugated Steel Plate Retaining Walls

The mechanical performance of corrugated steel plate retaining walls is not only affected by the plate thickness, but the corrugation parameters (geometric characteristics such as corrugation height and corrugation pitch) also play a vital role in the structural stiffness, stress distribution, and soil–structure interaction. Different corrugation parameters directly affect the equivalent cross-sectional properties and flexural performance of the corrugated steel plate, thereby altering the deformation and mechanical response of the retaining wall under lateral earth pressure. In this section, by changing the corrugation types of the corrugated steel plate, the influence of five different corrugation dimensions (Corrugation Profile 1 to Corrugation Profile 5) on the horizontal displacement of the corrugated steel plate retaining wall, the settlement of the backfill behind the wall, and the stress of the retaining wall is studied, respectively. The focus is placed on the influence

law of the variation in corrugation height and corrugation pitch on the horizontal displacement, stress distribution, and overall stability of the retaining wall. By analyzing the deformation and stress results, the maximum horizontal deformation of the corrugated plate is controlled, and the most reasonable corrugation type for the corrugated plate retaining wall is obtained. The schematic diagram of the dimensions of the five different corrugation profiles is shown in Figure 12.

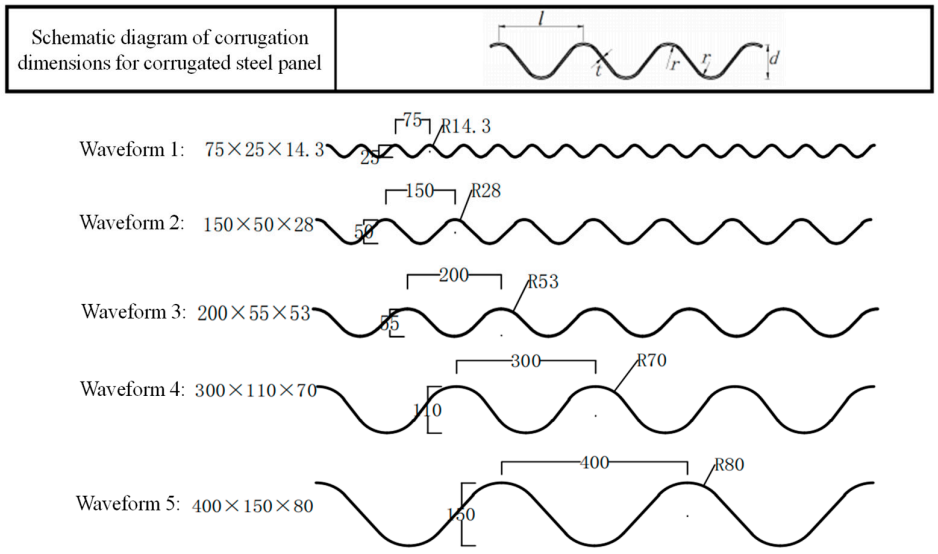

Figure 12. Schematic diagram of Corrugation Profiles 1 to 5.

3.3.1. Horizontal Displacements of Corrugated Steel Plate Retaining Walls

Figure 13 presents the contour plots of horizontal displacement of corrugated steel plate retaining walls with different corrugation dimensions. As shown in the figure, under the action of self-weight and lateral earth pressure, the horizontal displacement trends of corrugated steel plate retaining walls with different corrugation types are basically consistent, all presenting a bulging phenomenon characterized by an outward protrusion in the middle and lower parts and a contraction in the upper part. The horizontal displacement of the corrugated steel plate wall reaches approximately 123.28 mm for Corrugation Profile 1, and decreases sequentially to 103.74 mm, 84.98 mm, 70.33 mm, and 58.43 mm for Corrugation Profile 2 to Profile 5, respectively. Increasing the corrugation pitch from 75 mm to 400 mm and corrugation height from 25 mm to 150 mm reduces the maximum horizontal displacement by 52.6%. This demonstrates that larger corrugation profiles significantly improve structural stiffness. It can be seen that, from Corrugation Profile 1 to Corrugation Profile 5, with the increase in corrugation pitch and corrugation height, the overall horizontal displacement of the wall presents a significant decreasing trend.

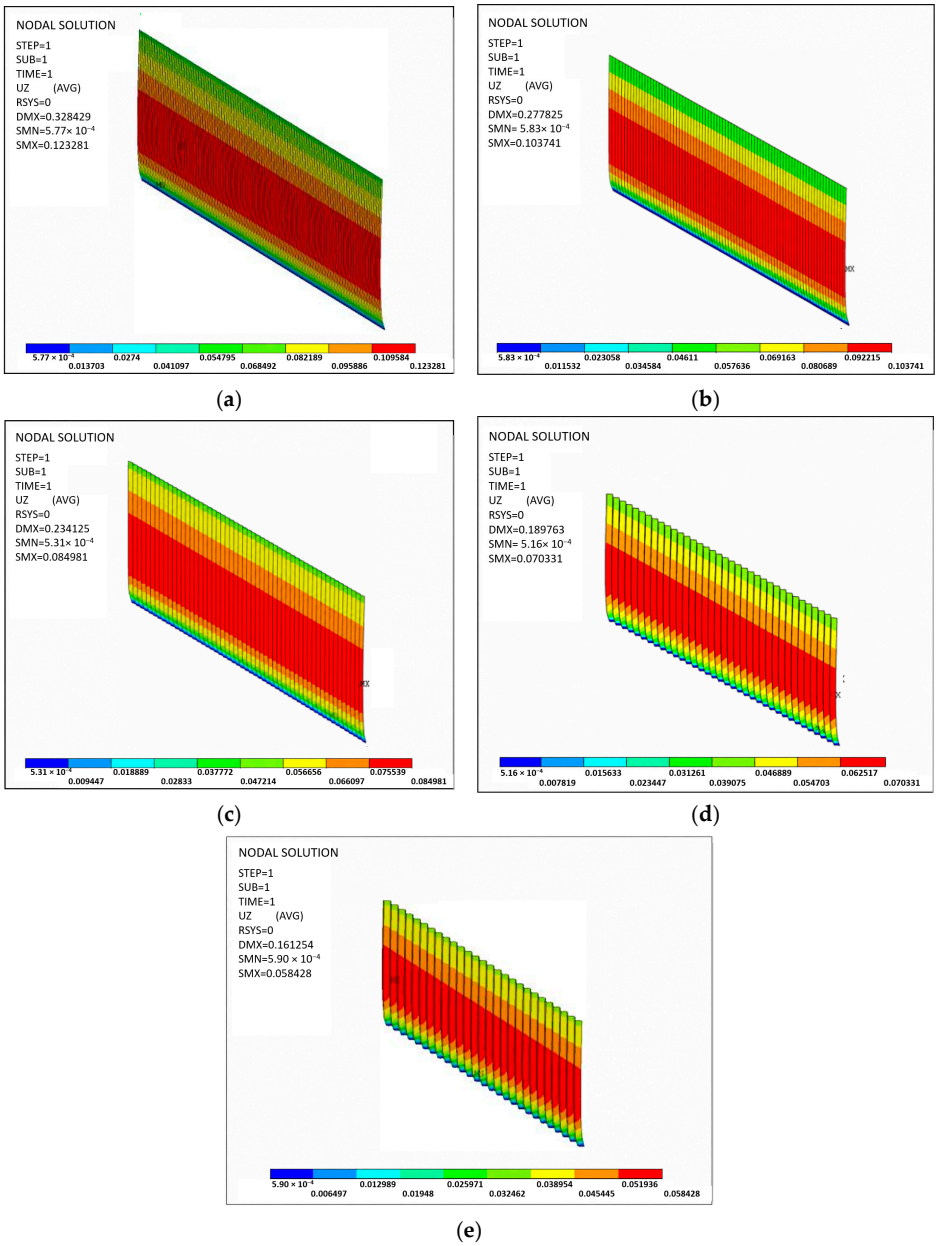

Figure 13. Contour plots of horizontal displacement of corrugated steel plate retaining walls with different corrugation profiles: (**a**) Corrugation Profile 1; (**b**) Corrugation Profile 2; (**c**) Corrugation Profile 3; (**d**) Corrugation Profile 4; and (**e**) Corrugation Profile 5.

Figure 14 presents the distribution curves of horizontal displacement along the wall height of the corrugated steel plate retaining wall under different corrugation profile conditions. It can be seen from the figure that the horizontal displacement distribution along the wall height of the corrugated steel plate retaining wall under different corrugation profile conditions generally presents a similar deformation mode. In terms of the corrugation parameters, as the corrugation profile gradually increases from Corrugation Profile 1 (l = 75 mm, d = 25 mm) to Corrugation Profile 5 (l = 400 mm, d = 150 mm), the overall horizontal displacement of the wall presents a significant decreasing trend. The specific performance is as follows: the displacement at the same height decreases significantly with the increase in corrugation profile. At the same height position, the horizontal displacement corresponding to Corrugation Profile 1 is the largest, followed by Corrugation

Profile 2 and 3, while that of Corrugation Profile 4 and 5 is the smallest. Larger corrugation profiles increase the section modulus of the steel plate, which significantly enhances the flexural stiffness. This explains why increasing the corrugation pitch and height reduces displacement more effectively than increasing plate thickness.

The increase in corrugation parameters (increase in l and d) significantly improves the cross-sectional moment of inertia and equivalent flexural stiffness of the corrugated steel plate, thereby enhancing the resistance of the wall to lateral earth pressure. Meanwhile, a larger corrugation height makes it easier for the corrugated plate to form a spatial stress state and arching effect, which is conducive to the redistribution of stress and deformation, and thus effectively restricts the development of horizontal displacement of the wall. Overall, increasing the corrugation pitch and corrugation height of the corrugated steel plate can significantly reduce the horizontal displacement of the retaining wall and improve the deformation performance of the structure. The reasonable selection of larger corrugation parameters is helpful to improve the overall stability and service safety of the corrugated steel plate retaining wall and provides a theoretical basis for the subsequent engineering optimization of corrugation parameters.

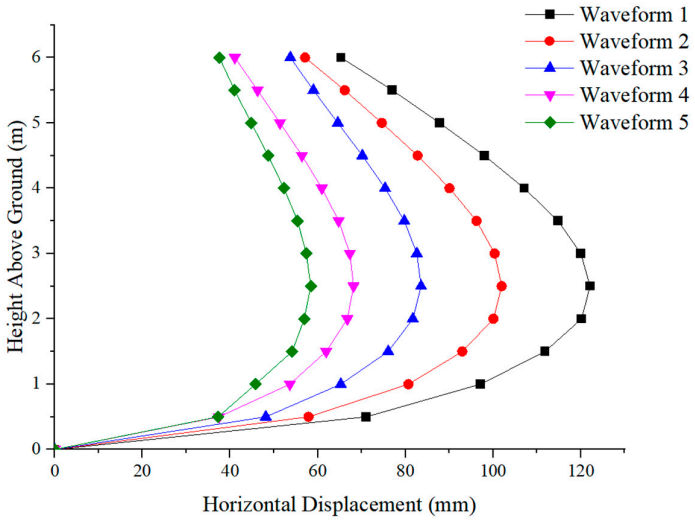

Figure 14. Horizontal displacement curves of corrugated steel plate retaining walls with different corrugation profiles.

3.3.2. Stress of Corrugated Steel Plate Retaining Walls

Figure 15 presents the equivalent stress for corrugated steel plate retaining walls with different corrugation dimensions. As shown in the figure, under the action of self-weight and lateral earth pressure, the equivalent stress trends of corrugated steel plate retaining walls with different corrugation dimensions are basically consistent. All walls exhibit the distribution characteristic of low stress in the upper section and high stress in the lower section, with the maximum stress occurring at the junction between the corrugated steel plate and the concrete foundation. The equivalent stress of the corrugated steel plate wall is approximately 52.7 MPa for Corrugation Profile 1, and increases sequentially to 53.3 MPa, 53.5 MPa, 54.9 MPa, and 57.6 MPa for Corrugation Profile 2 to Profile 5, respectively. The equivalent stress of the corrugated steel plate wall increases gradually from Corrugation Profile 1 to Corrugation Profile 5.

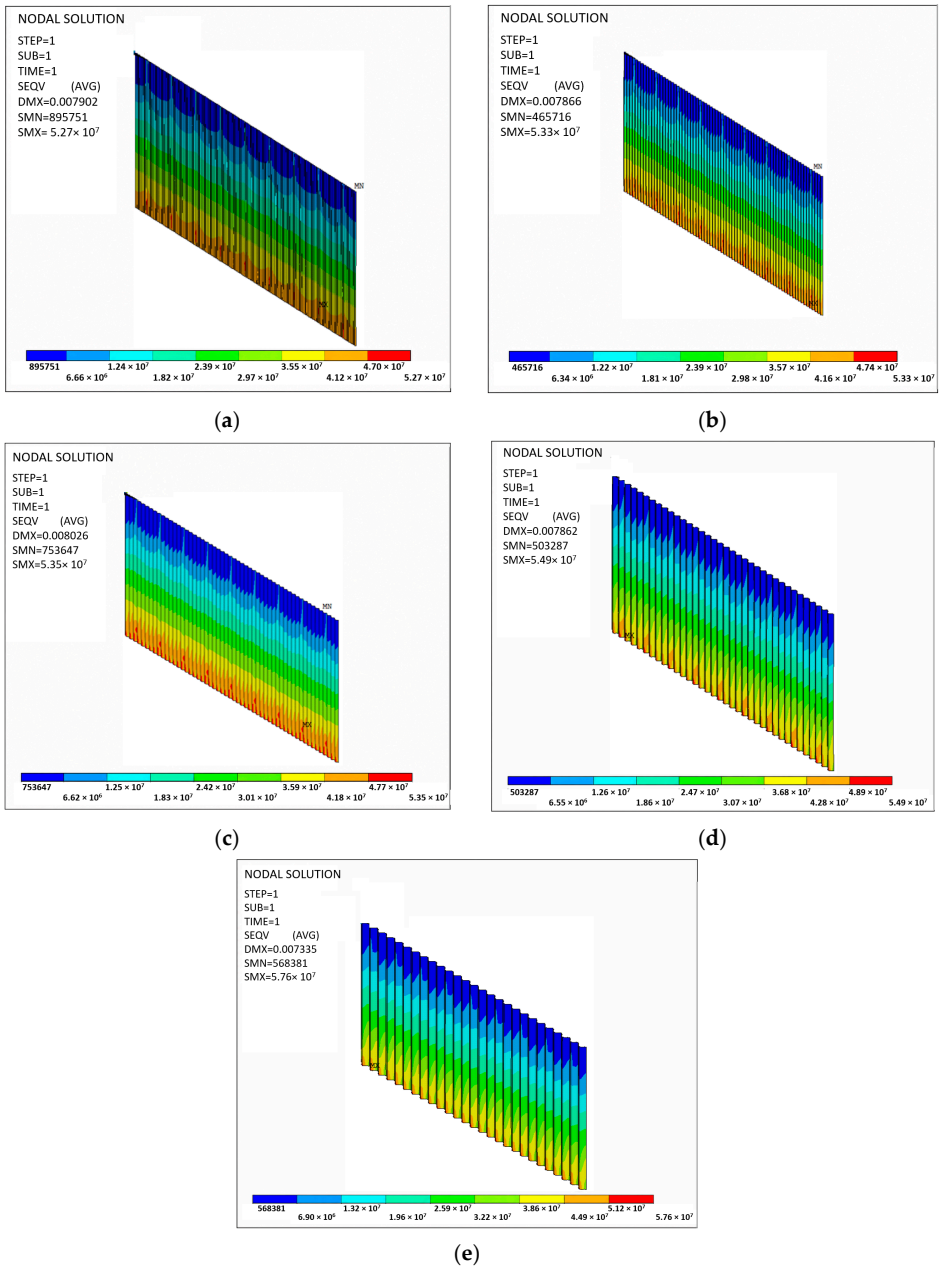

Figure 15. Contour plots of equivalent stress of corrugated steel plate retaining walls with different corrugation profiles: (**a**) Corrugation Profile 1; (**b**) Corrugation Profile 2; (**c**) Corrugation Profile 3; (**d**) Corrugation Profile 4; and (**e**) Corrugation Profile 5.

Figure 16 presents the distribution curves of equivalent stress along the wall height of the corrugated steel plate retaining wall under different corrugation profile conditions. The differences between different corrugation profiles are mainly reflected in the stress level and gradient variation in the middle–lower part and local upper sections of the wall. Corrugation Profile 1 presents relatively high stress points in the upper part, with a slightly larger dispersion of the overall curve. The stress distributions of Corrugation Profile 2, 3, and 4 are generally close, showing a consistent attenuation characteristic with the increase in wall height. Corrugation Profile 5 has an overall lower equivalent stress in most height ranges, especially in the middle–lower section, which reflects that the increase in corrugation parameters has a certain reduction effect on the stress level of the structure.

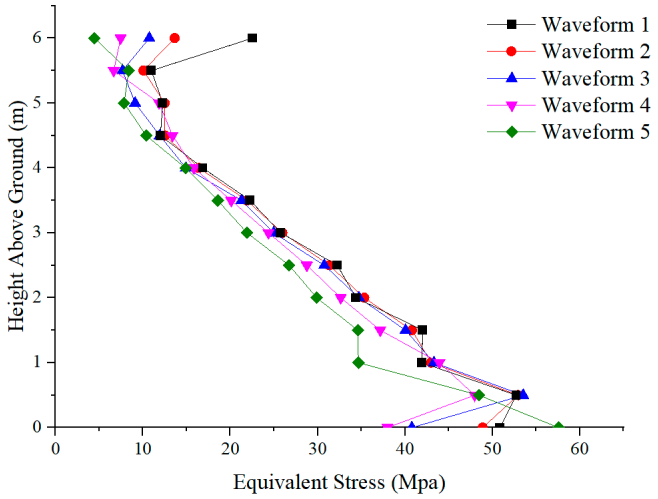

Figure 16. Equivalent stress curves of corrugated steel plate retaining walls with different corrugation profiles.

3.4. Influence of Different Tie Reinforcement Parameters on the Mechanical Performance of Prefabricated Corrugated Steel Plate Retaining Walls

The mechanical performance of prefabricated corrugated steel plate retaining walls depends not only on the geometric and material parameters of the wall face plate, but also on the cooperative mechanical behavior between the wall and the backfill behind the wall, which also plays a critical role. As an important load-bearing component connecting the wall and the soil, the layout spacing of tie reinforcements directly affects the lateral restraint capacity, internal force transfer path, and overall stability of the structure. It is a key design factor for controlling wall deformation and improving the bearing performance of the structure. The schematic diagram of the tie reinforcement layout is shown in Figure 17.

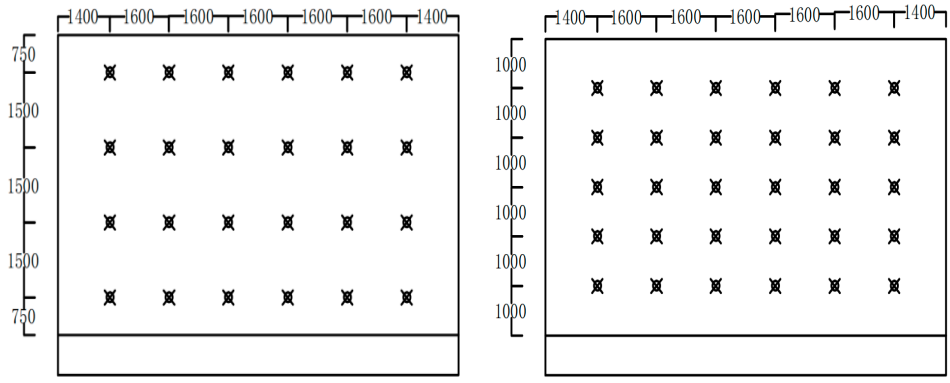

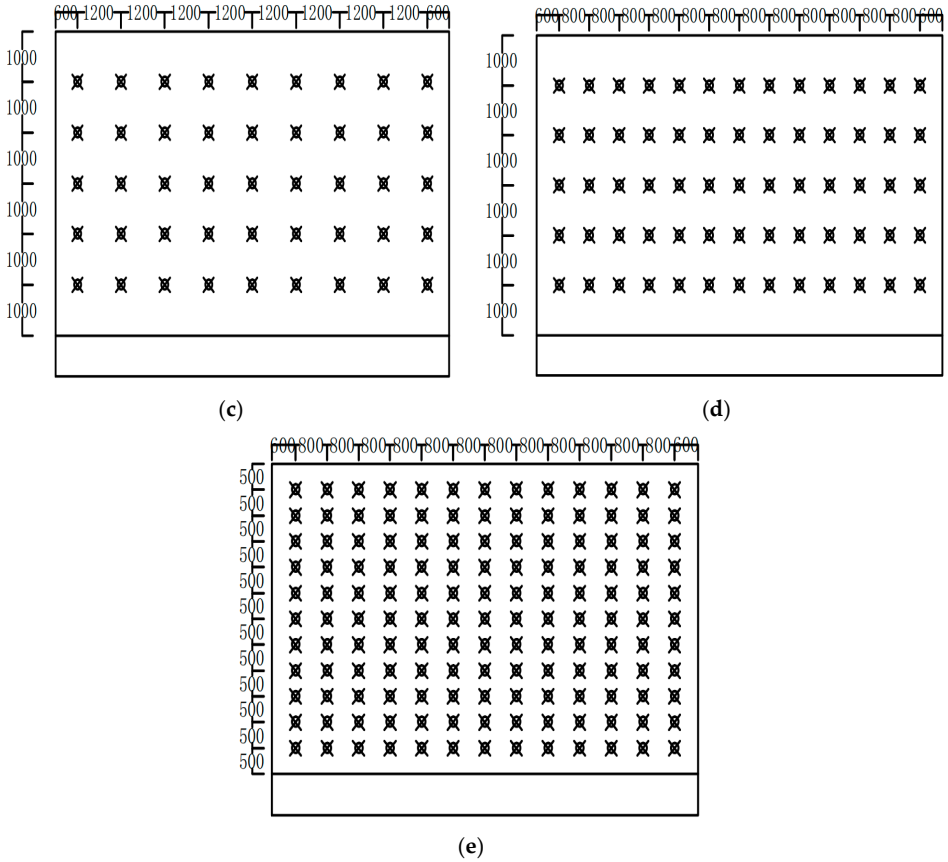

Figure 17. Schematic diagram of tie reinforcement layouts: (**a**) Tie Reinforcement Layout 1; (**b**) Tie Reinforcement Layout 2; (**c**) Tie Reinforcement Layout 3; (**d**) Tie Reinforcement Layout 4; and (**e**) Tie Reinforcement Layout 5.

3.4.1. Horizontal Displacements of Corrugated Steel Plate Retaining Walls

Figure 18 presents the horizontal displacement of corrugated steel plate retaining walls with different tie reinforcement layouts. As shown in the figure, under the action of self-weight and lateral earth pressure, the horizontal displacement trends of corrugated steel plate retaining walls with different tie reinforcement layouts are not completely identical. Although the main deformation trend still presents the bulging phenomenon, the concentration degree of horizontal displacement varies significantly. The horizontal displacement of the corrugated steel plate wall is approximately 75.10 mm for Tie Reinforcement Layout 1, and decreases nonlinearly and sequentially to 67.54 mm, 58.43 mm, 51.48 mm, and 36.88 mm for Tie Reinforcement Layout 2 to 5, respectively.

Figure 19 presents the horizontal displacement at the central position of the corrugated steel plate retaining wall under different tie reinforcement layout conditions. It can be seen from the figure that there are significant differences in the horizontal displacement distribution along the wall height of the corrugated steel plate retaining wall under different tie reinforcement spacing conditions. With the decrease in the longitudinal and transverse spacing of the tie reinforcements, the lateral displacement of the wall is significantly reduced, and the control effect on structural deformation is gradually enhanced.

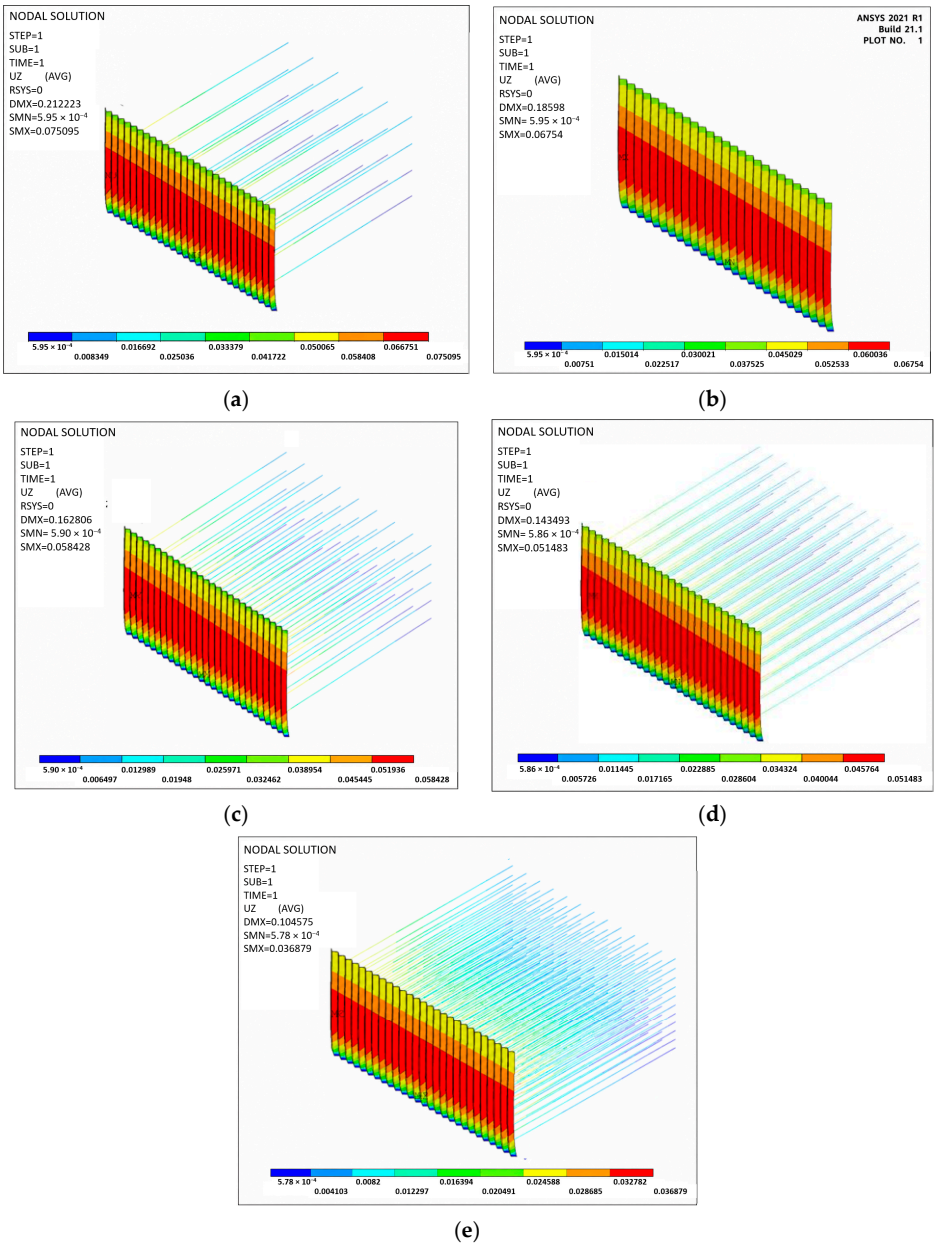

Figure 18. Contour plots of horizontal displacement of corrugated steel plate retaining walls with different tie reinforcement layout spacings: (**a**) Tie Reinforcement Layout 1; (**b**) Tie Reinforcement Layout 2; (**c**) Tie Reinforcement Layout 3; (**d**) Tie Reinforcement Layout 4; and (**e**) Tie Reinforcement Layout 5.

Under the condition of Tie Reinforcement Layout 1 (longitudinal spacing 1.5 m, transverse spacing 1.6 m), the retaining wall has the largest horizontal displacement, and the displacement curve shifts outward. This indicates that the restraint effect of the tie reinforcements is limited, the wall mainly relies on the inherent stiffness of the corrugated steel plate to resist earth pressure, and the lateral deformation is relatively significant. After reducing the longitudinal spacing to 1.0 m (Tie Reinforcement Layout 2), the overall displacement of the wall is reduced, indicating that increasing the vertical layout density of the tie reinforcements can effectively improve the overall stability of the wall. Under the condition of maintaining a longitudinal spacing of 1.0 m, a further reduction in the transverse spacing (Reinforcement Layouts 3 and 4) leads to a continuous decrease in the

horizontal displacement of the wall, with the displacement curves progressively retracting inward. This trend indicates that the synergistic interaction between the reinforcement strips and the backfill soil is enhanced, allowing the reinforcement to bear a greater proportion of the lateral earth pressure and thereby effectively restraining the lateral deformation of the wall. When Tie Reinforcement Layout 5 with a longitudinal spacing of 0.5 m and a transverse spacing of 0.8 m is adopted, the retaining wall has the smallest horizontal displacement within the full height range, and the displacement curve is the flattest, showing the optimal deformation control effect. Therefore, reducing both the longitudinal and transverse spacing of the tie reinforcements is helpful in reducing the horizontal displacement of the corrugated steel plate retaining wall. The reduction in longitudinal spacing plays a leading role in the overall deformation control, while the further reduction of transverse spacing can achieve a more significant displacement inhibition effect on this basis.

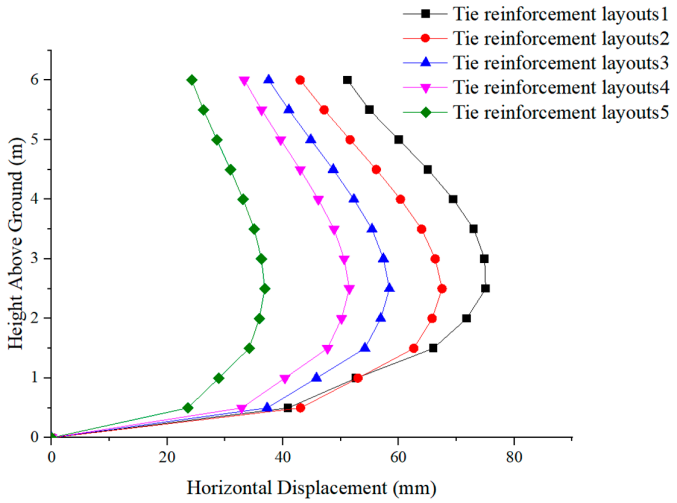

Figure 19. Horizontal displacement curves of corrugated steel plate retaining walls with different tie reinforcement layouts.

3.4.2. Stress of Corrugated Steel Plate Retaining Walls

Figure 20 presents the equivalent stress for corrugated steel plate retaining walls with different tie reinforcement layouts. As shown in the figure, under the action of self-weight and lateral earth pressure, the equivalent stress trends of corrugated steel plate retaining walls with different tie reinforcement layouts are basically consistent. All walls exhibit the distribution characteristic of low stress in the upper section and high stress in the lower section, with the maximum stress occurring at the junction between the corrugated steel plate and the concrete foundation. The maximum stress of the corrugated steel plate wall is approximately 48.7 MPa for Tie Reinforcement Layout 1, and increases sequentially to 52.7 MPa, 57.6 MPa, 67.7 MPa, and 109.0 MPa for Tie Reinforcement Layout 2 to 5, respectively, with all values complying with the limit requirements of the relevant specifications.

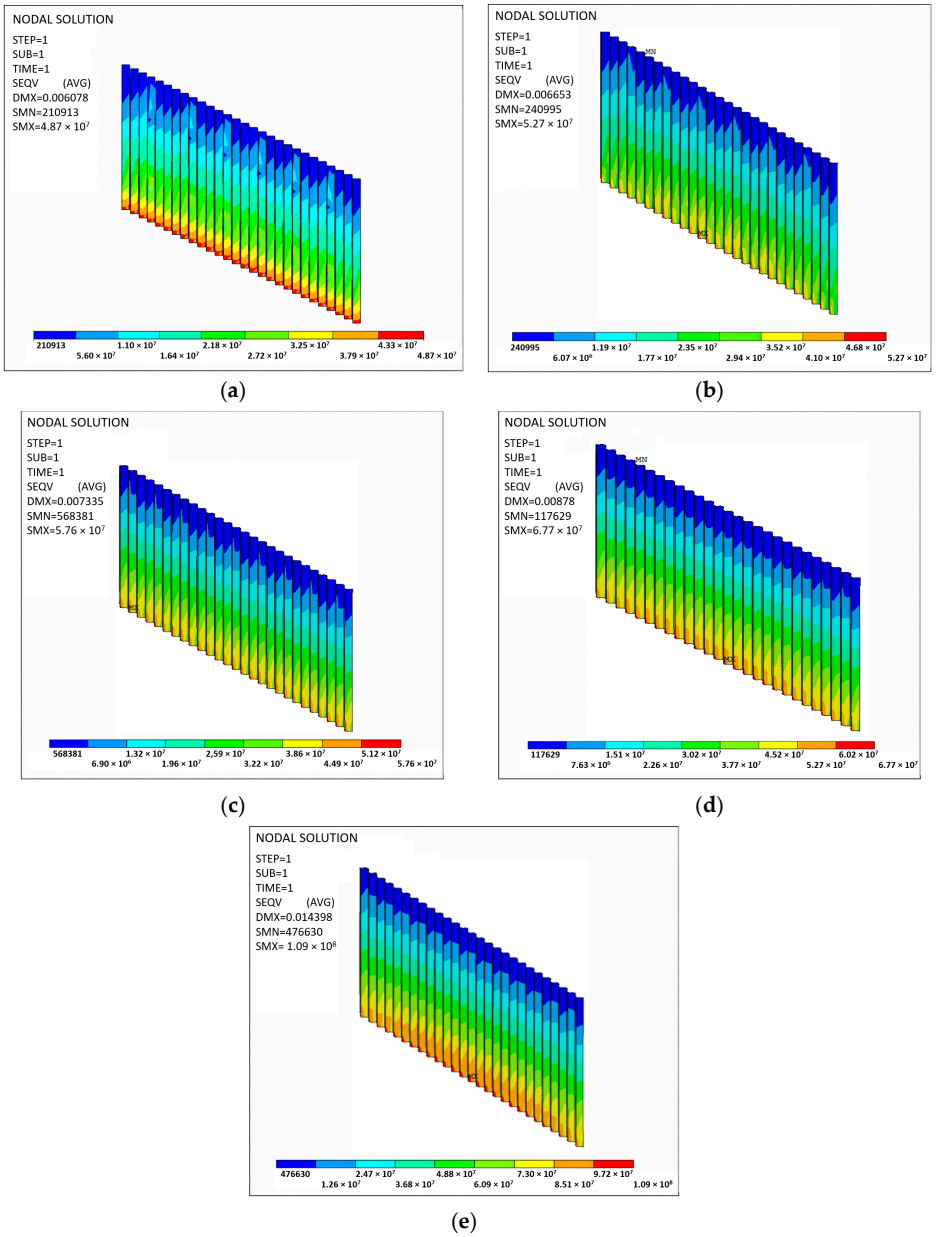

Figure 20. Equivalent stress contour plots of corrugated steel plate retaining walls with different tie reinforcement layout spacings: (**a**) Tie Reinforcement Layout 1; (**b**) Tie Reinforcement Layout 2; (**c**) Tie Reinforcement Layout 3; (**d**) Tie Reinforcement Layout 4; and (**e**) Tie Reinforcement Layout 5.

Figure 21 presents the equivalent stress curves at the central position of the corrugated steel plate retaining wall under different tie reinforcement layout conditions. It can be seen from the figure that different tie reinforcement layout schemes have a significant impact on the equivalent stress distribution of the corrugated steel plate retaining wall. Overall, with the reduction in the longitudinal and transverse spacing of the tie reinforcements, the equivalent stress level in the wall structure shows a significant increasing trend, and the stress distribution range gradually concentrates in the lower part of the wall. Under the condition of Tie Reinforcement Layout 1 (longitudinal spacing 1.5 m, transverse spacing 1.6 m), the overall equivalent stress level of the retaining wall is low, and the stress curve is close to the longitudinal axis as a whole. This indicates that the sharing effect of the tie reinforcements on the lateral earth pressure is limited at this time, the wall releases the internal force mainly through the overall displacement, and the structure has a

relatively small stress but a significant lateral deformation. When the longitudinal spacing is reduced to 1.0 m (Tie Reinforcement Layout 2), the overall equivalent stress of the wall is increased, especially in the middle and lower parts of the wall where the stress growth is more obvious. This illustrates that the increase in the number of tie reinforcements enhances the cooperative interaction between the wall and the backfill, allowing part of the lateral earth pressure to be borne by the tie reinforcements, thereby increasing the internal force level of the structure. Under the condition of maintaining a longitudinal spacing of 1.0 m, a further reduction in transverse spacing (Reinforcement Layouts 3 and 4) results in a continued increase in the equivalent stress of the wall. The stress curve shifts rightward as a whole, and the stress distribution becomes more continuous and uniform. This indicates that the increase in the layout density of the tie reinforcements effectively restricts the free deformation of the wall, and makes the structure gradually transform from a "deformation-dominated" state to a "stress-dominated" state. When Tie Reinforcement Layout 5 with a longitudinal spacing of 0.5 m and a transverse spacing of 0.8 m is adopted, the equivalent stress of the retaining wall reaches the maximum value, and the stress is mainly concentrated in the middle and lower parts of the wall. Under this layout scheme, the tie reinforcements form a relatively complete spatial reinforcement system, which significantly improves the overall stiffness of the structure. The lateral deformation of the wall is strongly constrained, and more earth pressure is reflected in the form of structural internal force. Therefore, the increase in the layout density of the tie reinforcements can effectively reduce the horizontal displacement of the wall, but, at the same time, led to a corresponding increase in the equivalent stress level of the corrugated steel plate. This indicates that there is a certain mutual restrictive relationship between the improvement in the structural deformation performance and the increase in the structural stress level caused by the layout of the tie reinforcements. Therefore, in engineering design, the deformation control requirements, material strength, and safety reserve should be comprehensively considered, and the longitudinal and transverse spacing of the tie reinforcements should be reasonably determined, so as to realize the coordination and unification of the safety and economy of the retaining wall structure.

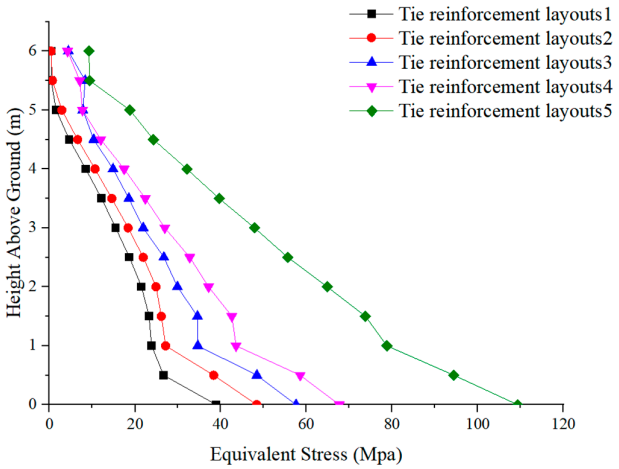

Figure 21. Equivalent stress curves of corrugated steel plate retaining walls with different tie reinforcement layouts.

4. Temperature Field of Prefabricated Corrugated Steel Plate Retaining Wall

In engineering projects of alpine permafrost regions, temperature action is one of the key factors affecting the long-term performance of structures. The construction site of the

retaining wall is located in western China, with typical continental climate characteristics, including a large annual temperature range, severe cold in winter, significant diurnal temperature variation, and frequent freeze–thaw cycles. The combined effect of these factors exposes the engineering structure to a complex temperature environment for a long time. For the prefabricated corrugated steel plate retaining wall, its structural form is a semi-exposed system: one side is directly affected by the atmospheric environment, and the other side is in contact with the backfill, forming an obvious non-uniform temperature field. Compared with traditional concrete retaining walls, corrugated steel plates have the characteristics of a high thermal conductivity and sensitive temperature response, and are more prone to additional stress and deformation under temperature changes. Therefore, it is necessary to conduct in-depth research on the distribution law of its temperature field. A transient temperature field analysis is established for prefabricated corrugated steel plate retaining walls applicable to alpine permafrost regions in this section. Based on this, a thermal–structure coupling analysis is conducted to reveal the temperature field distribution, systematically investigate the effect of temperature loads on the retaining wall, and specifically examine its temperature response characteristics under alpine permafrost conditions, as well as the resulting variations in equivalent stress and displacement. The findings aim to provide a more targeted theoretical basis for engineering design.

4.1. Variation Law of Temperature Field

Figure 22 presents the distribution characteristics of the temperature field variation in the corrugated steel plate retaining wall over an annual cycle. The contour plots reflect the magnitude of the temperature through color gradients, and the legend at the bottom defines the correspondence between temperature values and colors, which can intuitively reveal the spatial distribution and temporal evolution of the temperature within the retaining wall structure and the backfill behind the wall. On the whole, the temperature field of the corrugated steel plate retaining wall exhibits significant seasonal variation characteristics. From January to March and October to December, the surface temperature of the wall and backfill is generally below 0 °C, and the structure is in a frozen state. From April to September, the surface temperature gradually turns positive, and the soil enters the thawing stage, showing a typical freeze–thaw cycle process. Such periodic temperature variations not only affect the physical and mechanical properties of backfill soil, but also significantly influence the structural stress and deformation via the soil–corrugated steel plate interaction.

In January and February, the surface temperature at the top of the retaining wall reached −29.46 °C and −24.22 °C, respectively, as illustrated in Figure 22a,b. At this stage, cold has penetrated deep into the backfill behind the wall, resulting in a marked increase in the temperature gradient. The isotherms exhibit obvious bending near the corrugated steel plate, which indicates that the difference in thermophysical properties between the steel plate and the soil alters the local heat transfer characteristics. The frozen soil in this period features a high stiffness, which imposes a strong constraint on the corrugated steel plate. This constraint is conducive to restricting structural deformation, but may also induce a local additional stress concentration under the action of thermal stress. After entering March, as the air temperature rises, the temperature of the retaining wall system increases significantly compared with that in January and February, as shown in Figure 22c. In April, the surface temperature of the wall reaches 5.95 °C (Figure 22d), while the minimum temperature inside the backfill behind the wall remains at −12.81 °C. This indicates that only the surface soil layer has thawed, while the deep soil is still in a frozen state, resulting in a prominent “externally warm and internally cold” thermal characteristic of the structure. As time progresses, the surface temperature rises to 20.4 °C in May, whereas the minimum internal temperature is still −9.11 °C (Figure 22e). Heat is gradually

transferred into the deep soil, but the frozen layer has not completely disappeared. In June and July, the surface temperature of the wall reaches 29.97 °C and 31.67 °C, respectively (Figure 22f,g), hitting the annual peak values. This phenomenon is closely related to the intense solar radiation in the alpine regions of western China during summer. However, the minimum temperature inside the backfill at this stage remains at −6.51 °C and −4.69 °C, respectively, which demonstrates that the deep soil still maintains a sub-zero temperature state, thus forming a distinct non-uniform temperature field. This temperature distribution pattern of a "high temperature in the surface layer–low temperature in the interior" will induce the temperature-gradient-driven deformation of the corrugated steel plate, and simultaneously affect the distribution pattern of earth pressure. After entering August, the air temperature decreases gradually, the surface temperature of the wall drops back to 26.4 °C, and the minimum internal temperature rises to −3.44 °C, with the frozen layer further thinning, as presented in Figure 22h. By September, the surface temperature reaches 19.11 °C, and the minimum internal temperature is approximately −2.65 °C (Figure 22i). This indicates that the cold in the deep soil has not been completely released, and the soil is still in a near-frozen state, which provides the initial condition for the next freezing cycle. In October, the surface temperature of the retaining wall is approximately −5.29 °C (Figure 22j). As the temperature drops below the freezing point, the pore water in the backfill begins to freeze and release the latent heat of freezing, which slows down the temperature drop process. In November and December, the ambient air temperature decreases further, with the minimum wall surface temperature reaching −19.43 °C and −28.26 °C, respectively, as shown in Figure 22k,l. Cold is continuously transferred from the wall surface and ground surface into the interior of the backfill, the sub-zero temperature zone gradually expands to the deep soil, a frozen soil layer forms in the shallow backfill behind the wall, and the freezing depth increases continuously.

Under the climatic conditions of alpine permafrost regions, the temperature field of the corrugated steel plate retaining wall has the following characteristics. The temperature response of the wall and the surface layer of the backfill is rapid, while the temperature change in the deep layer shows significant hysteresis. The temperature presents a significant attenuation distribution along the depth direction, and the freeze–thaw action is mainly concentrated in the shallow layer of the backfill behind the wall. There is an obvious temperature gradient and isotherm bending phenomenon at the interface between the corrugated steel plate and the backfill, which is a temperature-sensitive area; long-term freeze–thaw cycles will cause the strength degradation and uneven deformation of the backfill, thus having a continuous impact on the internal force distribution and overall stability of the corrugated steel plate retaining wall. Therefore, in the engineering design of alpine permafrost regions, the coupling effect of hte temperature field variation and freeze–thaw effect on the structural performance of corrugated steel plate retaining walls should be fully considered, with particular attention paid to the mechanical response characteristics of the wall–soil interface and shallow backfill area.

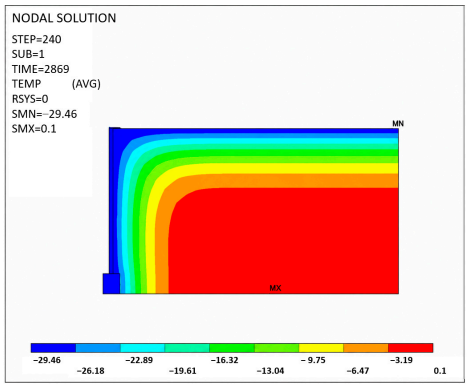
NODAL SOLUTION
STEP=240
SUB=1
TIME=2869
TEMP (AVG)
RSYS=0
SMN=−29.46
SMX=0.1
MN
MX
−29.46
−26.18
−22.89
−19.61
−16.32
−13.04
−9.75
−6.47
−3.19
0.1

(**a**)

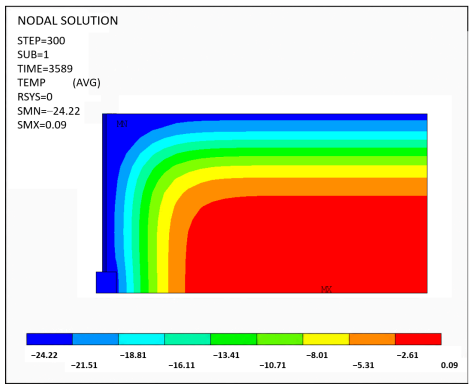
NODAL SOLUTION
STEP=300
SUB=1
TIME=3589
TEMP (AVG)
RSYS=0
SMN=−24.22
SMX=0.09
MN
MX
−24.22
−21.51
−18.81
−16.11
−13.41
−10.71
−8.01
−5.31
−2.61
0.09

(**b**)

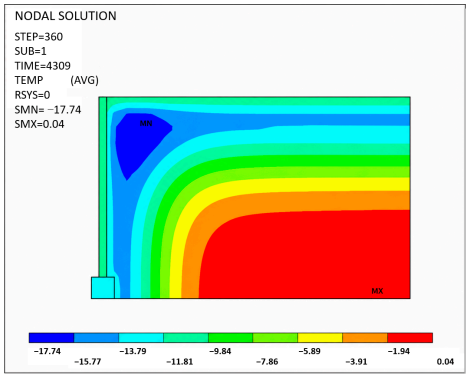
NODAL SOLUTION
STEP=360
SUB=1
TIME=4309
TEMP (AVG)
RSYS=0
SMN=−17.74
SMX=0.04
MN
MX
−17.74
−15.77
−13.79
−11.81
−9.84
−7.86
−5.89
−3.91
−1.94
0.04

(**c**)

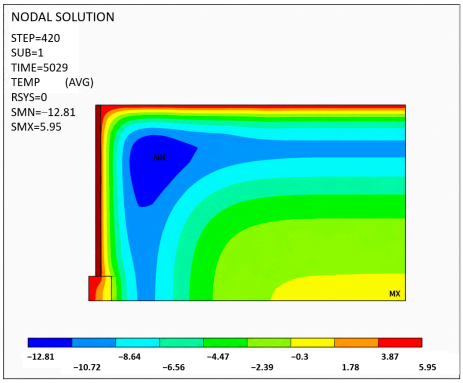
NODAL SOLUTION
STEP=420
SUB=1
TIME=5029
TEMP (AVG)
RSYS=0
SMN=−12.81
SMX=5.95
MN
MX
−12.81
−10.72
−8.64
−6.56
−4.47
−2.39
−0.3
1.78
3.87
5.95

(**d**)

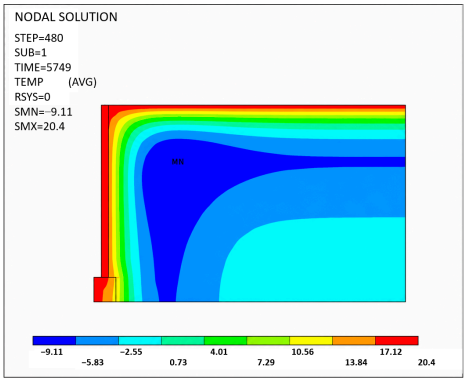
NODAL SOLUTION
STEP=480
SUB=1
TIME=5749
TEMP (AVG)
RSYS=0
SMN=−9.11
SMX=20.4
MN
−9.11
−5.83
−2.55
0.73
4.01
7.29
10.56
13.84
17.12
20.4

(**e**)

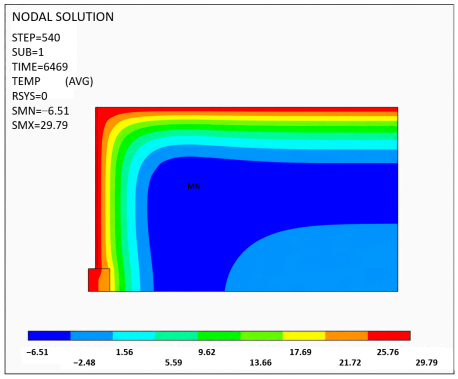
NODAL SOLUTION
STEP=540
SUB=1
TIME=6469
TEMP (AVG)
RSYS=0
SMN=−6.51
SMX=29.79
MN
−6.51
−2.48
1.56
5.59
9.62
13.66
17.69
21.72
25.76
29.79

(**f**)

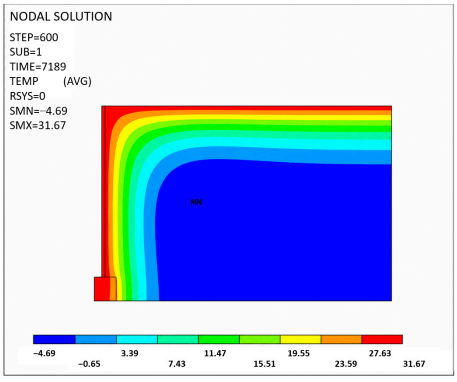
NODAL SOLUTION
STEP=600
SUB=1
TIME=7189
TEMP (AVG)
RSYS=0
SMN=−4.69
SMX=31.67
MN
−4.69
−0.65
3.39
7.43
11.47
15.51
19.55
23.59
27.63
31.67

(**g**)

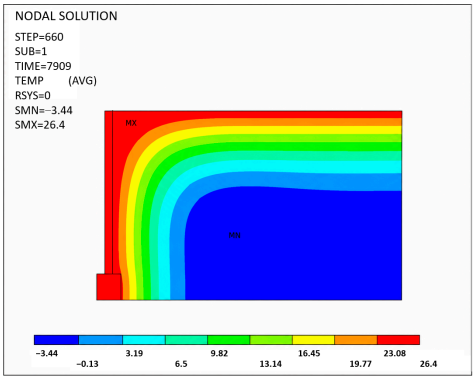
NODAL SOLUTION
STEP=660
SUB=1
TIME=7909
TEMP (AVG)
RSYS=0
SMN=−3.44
SMX=26.4
MX
MN
−3.44
−0.13
3.19
6.5
9.82
13.14
16.45
19.77
23.08
26.4

(**h**)

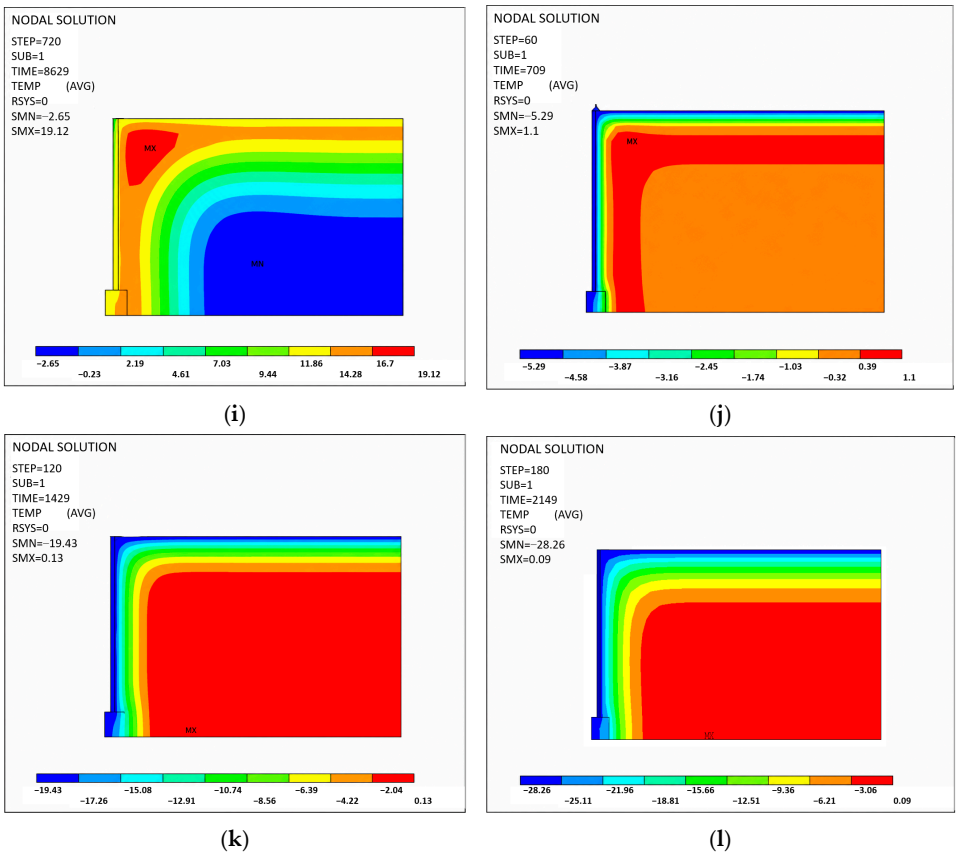

Figure 22. Contour plots of temperature field distribution of the corrugated steel plate retaining wall from January to December: (**a**–**l**) January to December.

4.2. Horizontal Displacements of Corrugated Steel Plate Retaining Walls Considering Temperature Effects

The initial temperature state and the typical condition after 12 months of freeze–thaw cycles are selected for a comparative analysis of the horizontal displacement contour plots of the corrugated steel plate retaining wall, to systematically study the influence of temperature field action on the structural deformation. The contour plots of horizontal displacement of the corrugated steel plate retaining wall are shown in Figure 23. It can be seen from the figure that, in terms of the overall displacement level, the maximum horizontal displacement of the retaining wall at the initial state is approximately 58 mm, while, after 12 months of freeze–thaw cycles, the maximum horizontal displacement increases to about 87 mm, an increase of nearly 50%. This result indicates that, under the environmental conditions of alpine permafrost regions, the temperature field has a significant amplification effect on the deformation of the corrugated steel plate retaining wall. Ignoring the temperature effect in the design stage may underestimate the actual horizontal displacement of the structure, thus compromising the engineering safety. In terms of the displacement distribution, the deformation modes of the wall under the two conditions are generally consistent, both presenting a typical bulging phenomenon. Specifically, the horizontal displacement is large in the wall top and middle–upper area, while small at the wall bottom, and the bulging position is approximately at one-third of the wall height. This is mainly because the bottom of the retaining wall is connected to the foundation with strong constraints, while the upper structure has weak constraints and is more prone to deformation under the combined action of earth pressure and temperature. Therefore, the structure presents similar deformation characteristics at different temperature stages.

However, with the extension of the action time of the temperature field, the displacement contours expand significantly towards the interior of the wall, the range of the high-displacement area (red area in the figure) increases remarkably, and the displacement growth is particularly significant in the middle and middle–lower areas of the wall. This indicates that the temperature effect not only increases the displacement amplitude, but also changes the relative distribution of displacement in the structure.

The influence of the temperature field on the displacement of the retaining wall is mainly reflected in two aspects: the thermal expansion and contraction effect, and freeze–thaw cycle action. The freeze–thaw cycle of the soil has an extremely critical impact on the deformation of the retaining wall. In winter, the air temperature decreases, the backfill behind the wall freezes, and pore water freezes to induce volume expansion, thereby generating frost heaving force, which forms an additional lateral thrust on the wall and increases the outward displacement of the wall. In summer, when the air temperature rises, the frozen soil thaws, the soil strength decreases, and the structural constraint is weakened, making the wall more prone to large deformation. Under the repeated action of annual periodic temperature changes, this irreversible deformation accumulates gradually, leading to a continuous increase in the overall displacement of the wall. The alternating action of "frost heaving thrust in winter and thaw settlement release in summer" makes the horizontal displacement of the wall present a trend of cumulative growth year by year, which is the fundamental reason for the significant increase in displacement after 12 months. Although the temperature field action does not alter the fundamental deformation mode of the corrugated steel plate retaining wall, it significantly amplifies the structural displacement and enlarges the extent of the high-displacement zone. Freeze–thaw cycles serve as the dominant factor driving the continuous increase in the displacement of the structure. Therefore, in the design of retaining walls in alpine permafrost regions, the coupling effect of the temperature load and freeze–thaw effect should be fully considered. By optimizing the structural form, reasonably arranging the tie reinforcement and anchoring measures, and selecting a low frost-heaving fill, the deformation of the wall can be effectively controlled, and the long-term stability of the structure can be ensured.

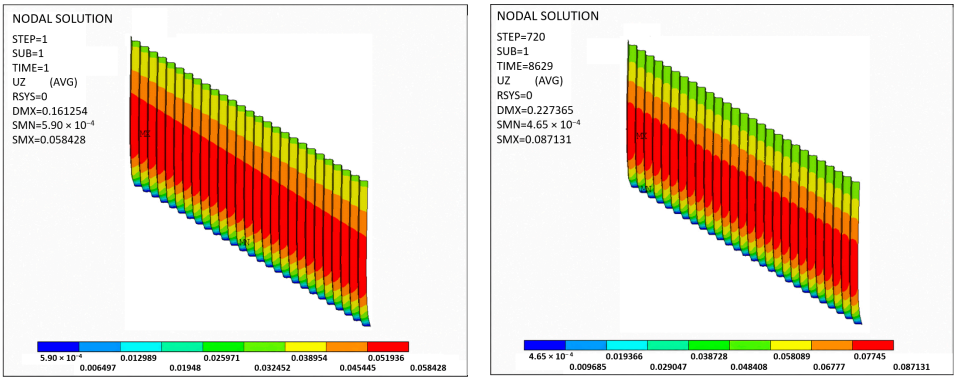

(**a**) (**b**)

Figure 23. Contour plots of horizontal displacement of the corrugated steel plate retaining wall: (**a**) initial displacement contour plot; and (**b**) displacement contour plot after 12 months.

4.3. Equivalent Stress of Corrugated Steel Plate Retaining Walls Considering Temperature Effects

Under the environmental conditions of alpine permafrost regions, the periodic change in the temperature field will not only induce structural deformation, but also have a significant impact on the internal stress distribution of the structure. Therefore, on the basis of completing the analysis of the temperature field and displacement response, it is necessary to further study the variation law of the equivalent stress of the corrugated steel

plate retaining wall under temperature action, to comprehensively reveal the influence mechanism of the temperature field on the mechanical performance of the structure. The contour plots of the equivalent stress of the corrugated steel plate retaining wall are shown in Figure 24. It can be seen from the figure that, under the initial temperature state, the overall stress distribution of the retaining wall is relatively stable, and the stress is mainly concentrated in the middle–lower part of the wall and the area near the foundation connection. This is because the wall undergoes bending deformation under the action of earth pressure, and the bottom has strong constraints, resulting in a large stress concentration in this area, while the upper part of the wall has weak constraints and a relatively low stress level. In terms of the distribution form, the stress presents a trend of a gradual decrease from the bottom to the top along the wall height, which is consistent with the typical loading characteristics of corrugated steel plate retaining walls. After 12 months of freeze–thaw cycles, the equivalent stress distribution of the retaining wall has changed significantly. First, in terms of the numerical value, the maximum equivalent stress of the structure is higher than that in the initial state, and the overall stress level is increased. Compared with the initial state (57.6 MPa), the maximum equivalent stress increased by 56.9% to 90.4 MPa after 12 months of freeze–thaw cycles. Second, in terms of the spatial distribution, the range in the high-stress area is significantly expanded, from the original main concentration at the bottom of the wall to the middle area gradually, and even a continuously distributed high-stress zone appears in local areas. This indicates that, under the long-term action of the temperature field, the internal stress state of the structure is redistributed, and the degree of stress concentration is enhanced.

The influence of the temperature field on the equivalent stress mainly comes from the combined action of the thermal expansion and contraction effect and freeze–thaw cycles. On the one hand, the corrugated steel plate material is sensitive to temperature changes: it expands when the temperature rises and contracts when the temperature drops. Due to the constraints of the soil and connection conditions, this free deformation is restricted, thereby generating additional thermal stress inside the structure. With repeated temperature changes, this thermal stress is continuously superimposed, making the overall stress level of the structure gradually increase. On the other hand, the volume and mechanical properties of the backfill behind the wall change significantly during freeze–thaw cycles. In the winter freezing stage, the soil volume expands, generating an additional lateral frost heaving force on the wall, which significantly increases the structural stress. In the summer thawing stage, the soil strength decreases, the lateral support capacity is weakened, and the structure further adjusts the internal force distribution on the basis of the original deformation. During this repeated action, the wall is in an alternate loading and unloading state for a long time, leading to continuous stress redistribution and the gradual expansion to a wider range.

In addition, due to the non-uniform spatial distribution of temperature, there is an obvious temperature gradient inside the wall, and the degree of thermal expansion and contraction varies in different parts, thereby inducing an additional bending effect of the structure. This non-uniform deformation further aggravates the local stress concentration, making the stress growth in the middle area of the wall more significant. It can be seen from the stress contour plots after 12 months that the significant increase in stress level in the middle–lower area is exactly the result of the combined action of the temperature gradient and structural constraints.

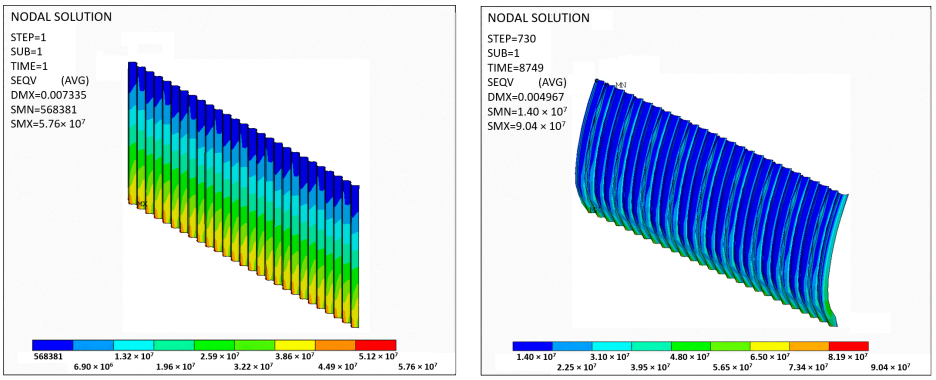

(**a**) (**b**)

Figure 24. Equivalent stress contour plots of the corrugated steel plate retaining wall: (**a**) initial equivalent stress contour plot; and (**b**) equivalent stress contour plot after the 12th month.

5. Discussion

To clearly demonstrate the originality and significance of this work, it is necessary to compare our findings with the existing literature in the field. The following Table 5 systematically compares the main research dimensions, representative studies, limitations of existing research, and contributions of this study.

Table 5. Comparison with existing literature.

Research Dimension	Representative Existing Studies	Limitations of Existing Research	Contributions of This Study
Application Environment of Corrugated Steel Structures	Beben et al. [2]: Static performance of corrugated steel bridges in temperate regions. Davis et al. [3]: Seismic response of buried corrugated metal pipes in normal soil conditions. Ji et al. [7]: Mechanical behavior of corrugated steel retaining walls at room temperature.	Almost studies focus on conventional non-frozen environments; none systematically investigates the performance of corrugated steel plate retaining walls in alpine permafrost regions with severe freeze–thaw cycles.	Comprehensive study on prefabricated corrugated steel plate retaining walls in alpine permafrost regions; quantified the significant amplification effect of freeze–thaw cycles (49.7% increase in displacement and 56.9% increase in stress after 12 months).
Retaining Structure Type in Permafrost Regions	Jiang et al. [20]: Thermal stability of concrete water retaining walls. Woo et al. [28]: Mechanical behavior of concrete retaining walls under frost heave. Guo et al. [21]: Corrugated steel–concrete composite support structures.	Research is dominated by traditional rigid concrete structures; very limited understanding of flexible corrugated steel structure–soil interaction in frozen soil.	Revealed the cooperative working mechanism between flexible corrugated steel plates and frozen soil; the variation patterns in displacement and stress of corrugated steel retaining walls under freeze–thaw environment were investigated.
Parameter Optimization for Cold Regions	Das et al. [12]: Multi-objective optimization of concrete retaining walls for general conditions. Kayabekir et al. [14]: Eco-friendly design methods for conventional retaining walls. DB63/T 1850-2020 [29]: General design specifications for corrugated steel retaining walls.	Previous optimization studies do not account for the special environmental effects of alpine permafrost; existing specifications lack quantitative design parameters for extreme cold regions.	Provided environment-specific quantitative design parameters (wall thickness, corrugation profile, and tie reinforcement spacing) and a 50% safety margin recommendation for freeze–thaw effects.

Temperature Field Coupling Effect	Xiao et al. [30]: Temperature distributions in geogrid-reinforced soil walls. Huang et al. [31]: Temperature distribution of composite box-girders with corrugated steel webs.	Temperature effect studies focus on temperature distribution rather than structural mechanical response; no quantitative analysis of thermal stress contribution in steel retaining walls.	Quantified the temperature field effects on the structural response in alpine permafrost regions; indicates that temperature effects are a critical control factor that must be explicitly considered in the design of retaining walls in alpine permafrost regions.

To thoroughly elucidate the mechanism by which parameter variations affect the structural response, this study conducts a quantitative analysis of the observed nonlinear behaviors from the perspective of system stiffness. A corrugated steel plate retaining wall is a cooperative load-bearing system composed of corrugated steel plate facing, tie reinforcements, and backfill soil, where the overall mechanical response is governed by the stiffness matching among the three components rather than the stiffness of any single element: (1) the facing provides the primary bending and shear resistance to control the global wall deformation; (2) the tie reinforcements offer horizontal restraint and transmit earth pressure to the stable soil behind; and (3) the backfill soil supplies passive resistance to complete the integrated load-bearing system.

Based on the comprehensive analysis of the field test data and thermo-mechanical coupling numerical simulation results, we found that the high thermal conductivity of corrugated steel (52 W/(m·°C)) creates significantly steeper temperature gradients at the wall–soil interface compared to traditional concrete structures (thermal conductivity 2 W/(m·°C)). During rapid temperature changes in alpine regions, the steel plate expands or contracts much faster than the adjacent frozen soil, but this free deformation is severely constrained by the surrounding soil and rigid foundation connections, generating substantial additional thermal stress within the structure. The inherent flexibility of corrugated steel plates allows for a partial adaptive deformation to soil frost heave, reducing peak structural stresses by approximately 18% compared to rigid concrete retaining walls under identical frost heave conditions. This is a unique advantage of flexible steel structures in permafrost regions, as it can effectively mitigate the destructive effects of uneven frost heave that often cause cracking and failure in rigid concrete structures.

6. Conclusions

This study focuses on the structural performance and parameter optimization of prefabricated corrugated steel plate retaining walls in alpine permafrost regions of western China. A validated finite element model combined with field test data was used to systematically investigate the effects of key design parameters and the temperature field on structural deformation and internal force. The main conclusions are as follows:

6.1. Core Quantitative Findings

(1) The established finite element model shows excellent agreement with the field test data, with all relative errors within the acceptable range (<20%) for engineering numerical simulation.

(2) When the plate thickness increases from 4 mm to 9 mm, the horizontal displacement of the retaining wall continuously decreases, but the reduction gradually narrows. Specifically, when the thickness increases from 4 mm to 5 mm, the displacement decreases by 33.13%; when further increased to 6 mm, it decreases by an additional 18.08%; thereafter, each 1 mm increment yields reductions of 8.32%, 7.65%, and 7.11%,

respectively. This indicates that, once the plate thickness exceeds 6 mm, the gain in displacement control from further thickening diminishes significantly.

(3) Increasing the corrugated steel plate thickness effectively reduces the structural horizontal displacement and equivalent stress, but the improvement effect gradually diminishes beyond a critical thickness. For typical engineering conditions with wall heights of 6 m in alpine permafrost regions, a 6 mm-thick Q235 steel plate is recommended. This thickness balances deformation control (maximum horizontal displacement < 60 mm, meeting the serviceability limit state requirement) and economic efficiency. For walls higher than 6 m, the plate thickness should be increased to 7–8 mm.

(4) Increasing the corrugation pitch from 75 mm to 400 mm and corrugation height from 25 mm to 150 mm reduces the maximum horizontal displacement by 52.6%. This demonstrates that larger corrugation profiles significantly improve the structural stiffness.

(5) The optimal tie reinforcement layout for 6 m-high walls is a 1.0 m longitudinal spacing and a 1.2 m transverse spacing. This configuration restricts the maximum horizontal displacement to 58.4 mm while keeping the equivalent stress at 57.6 MPa, which is well below the yield strength of Q235 steel (235 MPa). For walls higher than 6 m, the spacing should be reduced to 0.8 m × 1.0 m to provide additional lateral restraint.

(6) Temperature field effects significantly amplify the structural response in alpine permafrost regions. After 12 months of freeze–thaw cycles, the maximum horizontal displacement increases by 49.7% and the maximum equivalent stress increases by 56.9% compared to the initial state. This indicates that temperature effects are a critical control factor that must be explicitly considered in the design of retaining walls in alpine permafrost regions.

6.2. Practical Engineering Design Recommendations

Based on the research findings, the following specific design guidelines are proposed for prefabricated corrugated steel plate retaining walls in alpine permafrost regions:

(1) For wall heights ≤ 6 m: Use the 6 mm-thick Q235 steel plate, 400 mm × 150 mm corrugation profile, and tie reinforcement with 1.0 m longitudinal spacing and 1.2 m transverse spacing.

(2) For wall heights > 6 m: Increase the plate thickness to 7–8 mm and reduce the tie reinforcement spacing to 0.8 m × 1.0 m to control the deformation and stress.

(3) Incorporate a 50% safety margin for displacement and stress in the design to account for long-term freeze–thaw effects.

(4) Use well-graded gravel as backfill material to minimize frost-heave-induced additional loads.

6.3. Limitations and Future Research Needs

This study has several limitations and future research needs, which are specifically summarized as follows:

(1) Long-term material degradation: The present study focuses primarily on the structural response within the design stage and freeze–thaw loading period. Long-term material aging effects, including the stiffness degradation of steel components and the gradual deterioration of soil mechanical properties under repeated freeze–thaw cycles, were not explicitly considered.

(2) Corrosion effects: Although corrugated steel plates are typically protected by galvanization or weathering steel treatments, potential corrosion under long-term

exposure to moisture, deicing salts, and aggressive environmental conditions may reduce structural durability. These effects were not included in the current numerical model.

(3) Freeze–thaw variability uncertainty: The thermal boundary conditions adopted in this study were derived from representative meteorological data. However, actual field environments may exhibit significant interannual variability in temperature, snow cover, groundwater conditions, and freeze–thaw intensity. Such uncertainties may influence the long-term structural response.

(4) Future research directions: Future studies will focus on integrating corrosion evolution models, long-term freeze–thaw degradation mechanisms, stochastic climate loading, and long-term field monitoring data into the thermo-mechanical coupling framework to improve the prediction accuracy and durability assessment of corrugated steel retaining walls in alpine permafrost regions.

Author Contributions: Conceptualization, W.C. and T.D.; methodology, T.D. , F.C. and L.M.; software, validation, B.L. and F.C.; writing—original draft preparation, X.J., Q.Z. and B.L.; writing—review and editing, Q.Z., Y.L., and F.C.; funding acquisition, W.C., L.M., Y.L., and Q.Z. All authors have read and agreed to the published version of the manuscript.

Funding: This research was funded by the National Natural Science Foundation of China (No. 52508570), the Open Fund of National Science Center for Earthquake Engineering (No. 2025KFB4008), the Urumqi Hongshan Talents Program (No. HSYCP2025-020), the Science and Technology Innovation Leading Talent Project under the Tianshan Talent Training Program (No. 2023TSYCLJ0056), the Science and Technology Project of Xinjiang Transportation Investment (Group) Co., Ltd. (XJJTZZB-FWCG-202401-0002), the Science and Technology Assistance to Xinjiang Project of Xinjiang Uygur Autonomous Region (2024E02035), Xinjiang Transportation Investment (Group) Co., Ltd. Science and Technology Project (XJJTKX-FWCG-202412-0803), and the "Tianshan Talents" Training Program—Young Science and Technology Top-notch Talents Project —Basic-level Science and Technology Backbone Talent Training (2024TSYCJC0053).

Data Availability Statement: The original contributions presented in this study are included in the article. Further inquiries can be directed to the corresponding author.

Conflicts of Interest: Authors Wei Chen, Ting Duan, Lianxia Ma, Fang Chen, and Qingtao Zheng were employed by the company Xinjiang Communications Construction Group Co., Ltd. The remaining authors declare that the research was conducted in the absence of any commercial or financial relationships that could be construed as a potential conflict of interest. The authors declare that this study received funding from the National Natural Science Foundation of China (No. 52508570), the Open Fund of National Science Center for Earthquake Engineering (No. 2025KFB4008), the Urumqi Hongshan Talents Program (No. HSYCP2025-020), the Science and Technology Innovation Leading Talent Project under the Tianshan Talent Training Program (No. 2023TSYCLJ0056), the Science and Technology Project of Xinjiang Transportation Investment (Group) Co., Ltd. (XJJTZZB-FWCG-202401-0002), and the Science and Technology Assistance to Xinjiang Project of Xinjiang Uygur Autonomous Region (2024E02035). The funder was not involved in the study design; the collection, analysis, and interpretation of the data; the writing of this article; or the decision to submit it for publication.

References

1. Ołdakowska, E. Flexible engineering structures from the corrugated metal sheets: Comparison of costs of solutions used in road building. *IOP Conf. Ser. Mater. Sci. Eng.* **2017**, *269*, 012034. https://doi.org/10.1088/1757-899x/269/1/012025.
2. Beben, D.; Mańko, Z. Static tests on road bridge made from steel corrugated plates. *Stahlbau* **2007**, *76*, 381–390. https://doi.org/10.1002/stab.200710041.

3. Davis, A.C.; Bardet, P.J. Responses of buried corrugated metal pipes to earthquakes. *J. Geotech. Geoenviron. Eng.* **2000**, *126*, 28–39. https://doi.org/10.1061/(asce)1090-0241(2000)126:1(28).
4. Hao, H.; Long, K.; Liu, W.; Guo, C. High-Temperature Resistance of Galvanized Steel Corrugated Panel Partitions in Inclined Shafts of Extra-Long Road Tunnels. *Fire Technol.* **2026**, *62*, 10. https://doi.org/10.1007/s10694-025-01839-2.
5. Maleska, C. Contact interactions between soil and a corrugated metal sheet in soil-shell structures under construction. *Stud. Geotech. Mech.* **2021**, *44*, 1–12. https://doi.org/10.2478/sgem-2021-0018.
6. Ji, X.; Liang, J.; Guo, K. Numerical analysis of force and deformation characteristics of reinforced steel corrugated sheet retaining wall. *IOP Conf. Ser. Earth Environ. Sci.* **2020**, *510*, 052087. https://doi.org/10.1088/1755-1315/510/5/052087.
7. Pandit, K.U.; Mondal, G.; Punera, D. Investigating the static, free vibration, and buckling responses of corrugated steel plate-made structures using efficient homogenization based FE modelling. *Structures* 2024, 70, 107643. https://doi.org/10.1016/j.istruc.2024.107643.
8. Xu, J.Q.; Xu, J.; Yang, X.; Yan, Z.; Li, H.; Wang, H.; Tan, L.; Fei, D.; Li, J.; Luo, Y. Elastic foundation beam solution of tensile flexible retaining wall. *Int. J. Steel Struct.* **2022**, *22*, 622–631. https://doi.org/10.1007/s13296-022-00594-2.
9. Tong, J.; Guo, Y. Elastic buckling behavior of steel trapezoidal corrugated shear walls with vertical stiffeners. *Thin-Walled Struct.* **2015**, *94*, 112–123. https://doi.org/10.1016/j.tws.2015.06.005.
10. Lu, X.; Zhang, F.; Qin, W.; Zheng, H.; Feng, D. Experimental investigation on frost heave characteristics of saturated clay soil under different stress levels and temperature gradients. *Cold Reg. Sci. Technol.* **2021**, *183*, 103190. https://doi.org/10.1016/j.coldregions.2021.103379.
11. Zhussupbekov, A.; Shakhmov, Z.; Tleulenova, G. Geotechnical problems on freezing ground soil and experimental investigation in Kazakhstan. *Sci. Cold Arid Reg.* **2017**, *9*, 331–334. https://doi.org/10.1201/9781003416753-34.
12. Das, M.R.; Purohit, S.; Das, S.K. Multi-objective optimization of reinforced cement concrete retaining wall. *Indian Geotech. J.* **2016**, *46*, 354–368. https://doi.org/10.1007/s40098-015-0178-y.
13. Kashani, A.R.; Gandomi, A.H.; Azizi, K.; Camp, C.V. Multi-objective optimization of reinforced concrete cantilever retaining wall: A comparative study. *Struct. Multidiscip. Optim.* **2022**, *65*, 262. https://doi.org/10.1007/s00158-022-03318-6.
14. Kayabekir, A.E.; Arama, Z.A.; Bekdaş, G.; Nigdeli, S.M.; Geem, Z.W. Eco-friendly design of reinforced concrete retaining walls: Multi-objective optimization with harmony search applications. *Sustainability* **2020**, *12*, 6087. https://doi.org/10.3390/su12156087.
15. Öztürk, T.H.; Dede, T.; Türker, E. Optimum design of reinforced concrete counterfort retaining walls using TLBO and Jaya algorithm. *Structures* **2020**, *26*, 285–296. https://doi.org/10.1016/j.istruc.2020.03.020.
16. Saribas, A.; Erbatur, F. Optimization and sensitivity of retaining structures. *J. Geotech. Eng. ASCE* **1996**, *122*, 649–656. https://doi.org/10.1061/(asce)0733-9410(1996)122:8(649).
17. Wen, C.-B.; Guo, Y.-L.; Zuo, J.-Q.; Zhao, X.-Y. Strength design of prefabricated corrugated steel plate shear walls under combined compression and shear loads. *J. Build. Eng.* **2023**, *65*, 105790. https://doi.org/10.1016/j.jobe.2022.105790.
18. Xu, P.; Wei, Y.; Yang, Y.; Zhou, X. Application of fabricated corrugated steel plate in subway tunnel supporting structure. *Case Stud. Constr. Mater.* **2022**, *17*, e01323. https://doi.org/10.1016/j.cscm.2022.e01323.
19. Zhao, H.; Lu, R.; Guo, J.-R.; Sun, L.-H.; Tao, M.-X. Numerical investigation and seismic performance evaluation of an innovative prefabricated structural system. *J. Constr. Steel Res.* **2024**, *223*, 109061. https://doi.org/10.1016/j.jcsr.2024.109061.
20. Jiang, H.; Liu, C.; Wang, E.; Liu, X.; Ren, Z.; Han, H. Numerical modelling of thermal stability for a water retaining wall in permafrost regions. *Therm. Sci. Eng. Prog.* **2022**, *36*, 101494. https://doi.org/10.1016/j.tsep.2022.101494.
21. Guo, C.; Wang, Z.; Zhao, H.; Zhou, Z.; Wang, M. Numerical simulation of corrugated steel concrete prefabricated support structure for underground engineering. *Sustainability* **2023**, *15*, 14495. https://doi.org/10.3390/su151914495.
22. Li, K.; Zhu, L.; Xiong, F.; Liu, J.; Xue, Y.; Cao, Z.; Zhou, Y.; Liang, X.; Ji, M.; Liu, G.; et al. Review on Thermal Stimulation in Deep Geothermal Reservoirs: Thermo-Mechanical Mechanisms and Fracture Evolution. *Processes* **2026**, *14*, 1199. https://doi.org/10.3390/pr14081199.
23. Teng, T.; Wang, Y.; Ren, C.; Chen, Y. Modelling and simulation on anisotropic non-Darcy seepage characteristics of gas in naturally fractured coal. *Geomech. Energy Environ.* **2026**, *46*, 100828. https://doi.org/10.1016/j.gete.2026.100828.
24. *JTG 3363-2019*; Specifications for Design of Foundation of Highway Bridges and Culverts. China Ministry of Transport: Beijing, China, 2019.
25. *GB/T 700-2006*; Carbon Structural Steels. General Administration of Quality Supervision, Inspection and Quarantine of China, Standardization Administration of China: Beijing, China, 2006.

26. *GB/T 1591-2018*; High-Strength Low-Alloy Structural Steels, General Administration of Quality Supervision, Inspection and Quarantine of China, Standardization Administration of China: Beijing, China, 2018.
27. *GB/T 4171-2008*; Atmospheric corrosion resisting structural steel, General Administration of Quality Supervision, Inspection and Quarantine of China, Standardization Administration of China: Beijing, China, 2008.
28. Woo, H.J.; Go, G.H. Mechanical behavior assessment of retaining wall structure due to frost heave of frozen ground. *Int. J. Geo-Eng.* **2024**, *15*, 7. https://doi.org/10.1186/s40703-024-00210-8.
29. *DB63/T 1850-2020*; Design Specification for Highway Corrugated Steel Plate Retaining Walls. Qinghai Provincial Market Supervision Administration: Xining, China, 2020.
30. Xiao, C.; Cui, F.; Ding, L.; Wang, F.; Tian, W. Temperature Distributions in Geogrid-Reinforced Soil Retaining Walls Subjected to Seasonal Freeze–Thaw Cycles. *Int. J. Geomech.* **2022**, *22*, 04022234. https://doi.org/10.1061/(asce)gm.1943-5622.0002595.
31. Huang, S.; Cai, C.; Zou, Y.; He, X.; Zhou, T.; Zhu, X. Experimental and numerical investigation on the temperature distribution of composite box-girders with corrugated steel webs. *Struct Control Health Monit.* **2022**, *29*, e3123. https://doi.org/10.1002/stc.3123.